Mangrove-Derived Organic and Inorganic Carbon Exchanges Between the Sinnamary Estuarine System (French Guiana, South America) and Atlantic Ocean

Ray Raghab, Gérard Thouzeau, Romain Walcker, Vincent Vantrepotte, Gerd Gleixner, Sylvain Morvan, Jeremy Devesa, Emma Michaud

JGR Biogeosciences

RESEARCH ARTICLE
10.1029/2020JG005739

Key Points:
- Dissolved and particulate carbon exchange fluxes were estimated in a mangrove dominated estuary, French Guiana coastal systems
- Mangroves are exporter of DOC and importer of DIC and POC that is contrast to previous simplification of mangrove-derived C export
- Distinctive sources of DOC, POC, and DIC were observed referring to specificity and dynamics of the Guianese coastal systems

Supporting Information:
- Supporting Information S1

Correspondence to:
R. Ray,
raghab.ray@aori.u-tokyo.ac.jp;
raghab.ray@gmail.com

Citation:
Ray, R., Thouzeau, G., Walcker, R., Vantrepotte, V., Gleixner, G., Morvan, S., et al. (2020). Mangrove-derived C exchanges with Atlantic Ocean. *Journal of Geophysical Research: Biogeosciences*, *125*, e2020JG005739. https://doi.org/10.1029/2020JG005739

Received 11 MAR 2020
Accepted 16 JUL 2020
Accepted article online 5 AUG 2020

Author Contributions:
Data curation: Raghab Ray, Gérard Thouzeau, Romain Walcker, Vincent Vantrepotte, Gerd Gleixner, Sylvain Morvan, Jeremy Devesa, Emma Michaud
Formal analysis: Raghab Ray, Romain Walcker, Vincent Vantrepotte, Gerd Gleixner, Sylvain Morvan, Jeremy Devesa, Emma Michaud
Funding acquisition: Raghab Ray, Gérard Thouzeau, Emma Michaud
Methodology: Raghab Ray, Gérard Thouzeau, Vincent Vantrepotte, Gerd Gleixner, Sylvain Morvan, Jeremy Devesa, Emma Michaud
Project administration: Raghab Ray, Gérard Thouzeau, Emma Michaud
Software: Raghab Ray, Romain Walcker, Sylvain Morvan
(continued)

Mangrove-Derived Organic and Inorganic Carbon Exchanges Between the Sinnamary Estuarine System (French Guiana, South America) and Atlantic Ocean

Raghab Ray[1,2], Gérard Thouzeau[1], Romain Walcker[3], Vincent Vantrepotte[4,5], Gerd Gleixner[6], Sylvain Morvan[5], Jeremy Devesa[1], and Emma Michaud[1]

[1]CNRS, Univ Brest, IRD, Ifremer, LEMAR, Plouzané, France, [2]Now at Department of Chemical Oceanography, Atmosphere and Ocean Research Institute, University of Tokyo, Tokyo, Japan, [3]EcoLab, Univ Toulouse, CNRS, INPT, UPS, Toulouse, France, [4]LOG, UMR 8187 CNRS, Univ Lille, ULCO, Univ du Littoral Côte d'Opale, Wimereux, France, [5]LEEISA, USR 3456 CNRS, Univ Guyane, Ifremer, Centre de recherche de Montabo, Guyane Française, France, [6]Department of Biogeochemical Processes, Max Planck Institute for Biogeochemistry, Jena, Germany

Abstract There is growing evidence that a substantial fraction of the dissolved organic and inorganic carbon (DOC and DIC) and particulate organic carbon (POC) can be exported from mangroves to the ocean. Yet our understanding of C fluxes in mangrove forests is limited to only few regional studies that exclude the world's longest sediment dispersal system connected to the Amazon River. The present study aims at (1) examining tidal fluctuations of DOC, POC, and DIC; their isotopes; and optical properties such as chromophoric dissolved organic matter (CDOM) and (2) estimating their exchange fluxes between the mangroves and adjacent coastal water in the Sinnamary estuary, French Guiana. Time series observation highlighted that physical processes coupled to tides controlled diel dynamics and sources of DOC (e.g., litter leaching and pore water seepage) and POC (microphytobenthos, sediment resuspension, and bioturbation activities). Intense benthic remineralization could account for high water column pCO_2 and DIC exchange flux during the low tide. Mangrove-derived DOC export to inner shelf (8.14 g C m^{-2} day^{-1}) was exceeding import of POC and DIC from the mud bank and marine sources to the mangroves (1.35 and 0.90 g C m^{-2} day^{-1}, respectively). Because of specific dynamics of the Amazon mobile muds, local geomorphology, water column stratification, and environmental forcing, Guianese mangroves cannot be seen as simple C exporters to the Atlantic waters. These first data setting on C fluxes for the region should be included along with other studies to improve global mangrove C budget estimate.

1. Introduction

Mangroves are highly productive tidal wetlands, colonizing the margins between land and sea, occupying 0.5% of the coastal area and accounting for about 2.4% of tropical forests (Giri et al., 2011). Owing to their high productivity and tidal exchange with terrestrial and marine ecosystems, mangroves play a crucial role in the biogeochemical cycling of carbon and nutrients (Adame & Lovelock, 2011). Mangroves can sustain pelagic and benthic food webs, acting as nursery and exporting organic carbon (OC) forms, which are potential sources of energy for the aquatic organisms (Kristensen et al., 2008; Odum & Heald, 1975). Total C stock (also known as 'blue carbon') is strongly dependent on the magnitude of export or import of suspended sedimentary C and either marine or terrigenous organic matter, which is driven by the hydrodynamics (e.g., tidal regime, river flow, and rainfalls) and geomorphological settings (Lee et al., 2014; Woodroffe, 1992). However, uncertainties remain regarding the fate of the "blue carbon" due to lack of data on laterally driven dissolved inorganic carbon (DIC) component (piece of "missing carbon" in mangrove budget; Alongi, 2014; Bouillon et al., 2008).

The export of DOC and POC from mangroves to coastal sea has received considerable attention since past few decades, even though the limited number of quantitative studies still precludes an accurate assessment of OC export on a global scale (Dittmar et al., 2006; Jennerjahn & Ittekkot, 2002). Our understanding of OC export from the mangroves has developed from a relatively small number of quantitative estimates (<15; Call et al., 2019; de Rezende et al., 2007; Dittmar & Lara, 2001; Li et al., 2018; Maher et al., 2013; Ray,

Supervision: Raghab Ray, Gérard Thouzeau, Vincent Vantrepotte, Emma Michaud
Validation: Raghab Ray, Romain Walcker
Writing – review & editing: Raghab Ray, Gérard Thouzeau, Romain Walcker, Vincent Vantrepotte, Gerd Gleixner, Emma Michaud

Baum, et al., 2018; Santos et al., 2018; Taillardat et al., 2018; Twilley, 1985). Alternatively, reversed flux of POC, that is, inwelling from other sources, such as sea grass beds to the mangroves, was observed in few studies in Kenya, Arabian Gulf, and eastern Australia (Hemminga et al., 1994; Santos et al., 2018; Walton et al., 2014). Similar to OC, very few measurements were done to estimate the mangrove-derived DIC pool (Li et al., 2018; Maher et al., 2013; Miyajima et al., 2009; Santos et al., 2018; Sippo et al., 2016; Taillardat et al., 2018). This lack of sufficient quantitative estimates of mangrove-related DOC, POC, and DIC hampers generalizations regarding the role of mangroves as C source or sink for the adjacent oceans.

The coastline of French Guiana (FG hereafter) is characterized by fringing mangroves, which colonize on highly mobile mud banks originating from fine-grained sediment discharge of the Amazon River (754 ± 8.6 million tons year^{-1}; Anthony et al., 2010; Martinez et al., 2009). FG mangroves are suitable study sites for investigating C exchanges because the FG coast is potentially an important source of carbon due to the high standing tree biomass (Fromard et al., 1998; Walcker et al., 2018) and associated litter fall rates (Betoulle et al., 2001). Organic carbon is highly mobilized and mineralized by the suboxic conditions (Aller & Blair, 2006), tidal influence (Marchand, 2017), and bioturbation rates (Aschenbroich et al., 2016, 2017). Such OC products likely play an important role in biogeochemical exchanges with the Atlantic waters through retro-flexion of the Brazilian northern currents (Allison et al., 2000; Condie, 1991). Previous studies in the FG have demonstrated the role of mangroves and benthic microalgae as potential sources of DOC, POC, and DIC in the estuarine surface water (Gontharet et al., 2014; Ray, Michaud, et al., 2018), but C fluxes between the mangroves and coastal waters have yet to be quantified for this unique wetland region.

The present study aims to quantify seasonal and tidal variability of estuarine DOC, POC, and DIC and to estimate C exchange fluxes between the estuarine mangroves and FG coastal waters. Inferring the magnitude of such fluxes is challenging because the spatial and temporal complexity of FG estuaries may impede an accurate estimate of OC fluxes. Furthermore, data acquired in the present study could compare with other estuarine mangrove systems and contribute to the existing C budget for worldwide mangroves.

2. Material and Methods

2.1. Study Area

The study area is located in the mouth of the Sinnamary estuary, FG (Figure 1). The climate of FG is the subequatorial humid type with four seasons: a major "wet" season lasting from mid-April to early July when the Intertropical Convergence Zone (ITCZ) passes over French Guiana associated to trade winds northeasterly, and a major "dry" season lasting from August to November associated to relatively stable southeastern trade winds. Minor wet and dry seasons occur from late November to February and from March to April, respectively (Marchand et al., 2004). During this study, air temperature was in the ranges 25–27°C in June and 25.5–28.6°C in November 2015 (Météo France, http://www.meteofrance.gp), with maximum values between 12:30 and 16:30 and minimum at sunrise (6:30). Average rainfall recorded during the week of sampling in June and November was 10.5 and 2.1 mm/day, respectively. These rainfall data were retrieved from HY-SPLIT model, NOAA ARL database (http://www.arl.noaa.gov/ready.html).

The Sinnamary estuary is mesotidal to macrotidal, semidiurnal type, with spring and neap tide water levels up to 3.2 and 2.5 m above the hydrographic reference, respectively. River flow after the Petit Saut dam, upstream the Sinnamary estuary, varied between 700 and 193 $m^3\ s^{-1}$ during the study period in 2015 with maximum and minimum discharges found in June (wet season) and November (dry season), respectively (*source*: DEAL Guyane-EDF). Highest river flow during the first 2 weeks of June (500–700 $m^3\ s^{-1}$) was related to highest rainfalls in May and June (~638 mm in total; Météo France).

The Sinnamary estuary mud banks are colonized by mangrove stands of various ages. Sediment composition is dominated by muddy clay (~90%), originating from the Andes (Parra & Pujos, 1998), that migrates along the coast through successive depositional and erosional phases (1 to 5 km year^{-1}; Allison et al., 2000; Gardel & Gratiot, 2005). The Sinnamary shore mangroves are dominated by *Avicennia germinans* (Aschenbroich et al., 2016) associated with *Laguncularia racemosa* and *Rhizophora spp*. in the polyhaline estuarine area and along river sides toward the continent (Fromard et al., 2004; Proisy et al., 2009). Mangrove mapping (1–61 years stands) of the study area in 2015 allowed calculating that pioneer, young-pioneer, young, adult, and mixed or mature stands accounted for 36.4, 235.15, 302.01, 217.15, and 343.28 ha, respectively (1,134 ha

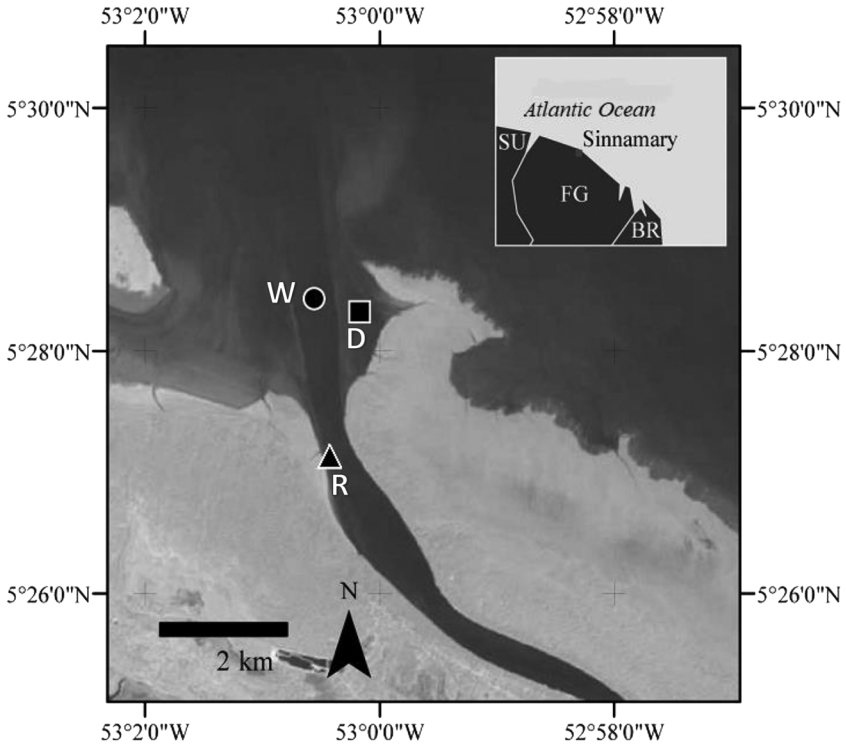

Figure 1. Location of sampling sites in June (wet season) and November (dry season) 2015. Time series sampling was carried out at Mooring Stations W in the river channel (June) and D close to the mangrove fringe area (November). R represents additional sampling station from the Sinnamary River in June and November. SU, FG, and BR represent Surinam, French Guiana, and Brazil (inset map).

in total), while bare mud surface area was 244.6 ha above 1.65 m from the hydrographic reference (Ray, Michaud, et al., 2018).

2.2. Study Sites and Sampling Periods

Field works were carried out in wet (1–9 June) and dry (10–20 November) seasons of 2015 during the neap tides. At spring tide, the flood condition lasts for about 4 to 5 hr and the subsequent ebb tide for 7 to 8 hr (Aschenbroich et al., 2017), but this dissymmetry disappears toward neap tide. The latter may favor maintaining the balance between material export and import within the estuary (i.e., exchange of C for this study). Time series were performed for 12 hr on 9 June (from 8:45 to 18:30; Figure 1, Site W) and for 24 hr on 18–19 November (tidal cycle starting at 10:30; Figure 1, Site D). It turned out in June that Site W, located in the river channel (>1.5 km from the mangroves), was exclusively influenced by freshwater inputs from the river. Following the June sampling results, Site D (located at 0.5 km from the mangrove) was chosen to better track the salinity variations with tide in surface water as well as the mangrove influence on water properties. Additional sampling was also performed near the mouth of the Sinnamary river (Salinity 0) at Site R located 1–2 km upstream from W and >2 km from D (Figure 1; see Ray, Michaud, et al., 2018).

2.3. Data Collection

2.3.1. Meteorological Records

Details of the field sampling are given in Table 1. A weather station (Davis Wireless Vantage Pro2, Hayward, CA, USA) mounted 3 m above the air-water interface and within ~200 m of the anchored boat recorded wind speed (m s^{-1}) and direction, humidity (%), air temperature (°C), and pressure (atm) on 5 min intervals in the dry season of 2015. By contrast, damage of the electronics did not allow recording meteorological data during the wet season. Atmospheric $pCO_{2(air)}$ (in ppm; 1 ppm signal noise at 370 ppm CO_2, calibration drift <0.4 ppm/°C at 370 ppm) was measured continuously ~2.5 m above surface water by a nondispersive infrared CO_2 gas analyzer (Li-COR LI-820) in both surveys.

Table 1
Details About the Sampling Periods, Sites Locations, Methodologies Applied, and Parameters Measured With Their Ranges of Variation During the Time Series Studies Performed in the Sinnamary estuary in June (wet) and November (dry) 2015

Date, Season, Duration, Tidal hrs.	GPS location and distance from mangroves	Continuous data loggers	Hourly sampling of biogeochemical parameters (surface water)	Observed ranges of basic water properties, meteorology, air CO_2
June 9, 2015 Wet season 12 hours	5°28′ 26″ N 53° 0′40″ W	ADCP: current speed YSI: water T, S, depth, turbidity, DO, Chl-a LI-COR: air pCO_2	Dissolved: DOC, TA, DIC, CDOM, ^{13}DOC, ^{13}DIC	Water T: 26.6-27.5 °C Current: 0.2-1.1 ms^{-1} Depth: 1.9-3.2m Surface S: 0-4.2
High tide: 10:05 Low tide: 16:24	~1.5 km from pioneer mangroves transition	Weather station: air T, wind speed, direction, pressure	Particulate: POC, PN, ^{13}POC, ^{15}PN, TSM, Chl-a, Pheo.	Air T: 24-26°C Wind: no data pCO_{2air}: 345-405 ppm
November 18-19, 2015 Dry season 24 hours	5°28′ 46″ N 53° 0′20″ W	ADCP portable: current speed (hourly) YSI: water T, S, depth, Turbidity, DO, Chl-a LI-COR: air pCO_2 WTW: S, pH (hourly)	Dissolved: DOC, TA, DIC, CDOM, ^{13}DOC, ^{13}DIC	Water T: 27.1-30 °C Current: 0.01-0.9 ms^{-1} Depth: 1.3-2.9 m Surface S: 4.7-25.4
High tide: 9:22, 21:44 Low tide: 15:35, 04:12	~0.5 km from Pioneer mangroves transition	Weather station: air T, wind speed, direction, pressure	Particulate: POC, PN, ^{13}POC, ^{15}PN, TSM, Chl-a, Pheo.	Air T: 25.5-28.6°C Wind: 1.3-7.3 ms^{-1} pCO_{2air}: 342-407 ppm

Note. Physical parameters were recorded continuously except for ADCP and WTW data (hourly basis). Water sampling in surface water was carried out hourly.

2.3.2. Water Physicochemical Records

Water depth, temperature, salinity, turbidity, and dissolved oxygen (DO) were recorded every minute with YSI probes 6920v2 (YSI Inc., Yellow Springs, OH, USA). In the wet season, the YSI probes were deployed at the surface (0.15 ± 0.03 m), at mid-depth (1.18 ± 0.39 m), and at different water depths (0.14 to 2 m) from 11:32 to 11:47 (early ebb), to record variations of the parameters according to depth (Table 2). In the dry season, YSI probes were deployed for continuous data recording in near-surface (0.44 ± 0.09 m) and bottom (1.55 ± 0.41 m) waters. Water current velocity was recorded with a moored Acoustic Doppler Current Profiler (ADCP@sontek) in the wet season (60 profiles with 20 layers from surface to bottom each hour) versus hand-held measurements by a flow probe (model FP111, Global Water) in the dry season (30 cm depth at each sampling time each hour).

2.3.3. Biogeochemical Parameters

At both sampling periods, water samples were collected every hour at ~0.3 m depth with acid-cleaned Nalgene bottles (1 L) to measure biogeochemical parameters plus water temperature and salinity. In the dry season, temperature (±0.1), salinity (±0.1), and pH (±0.002) were simultaneously measured directly in sampled overlying water and pore water, using a multiparameter water quality meter (WTW Multi 3500i, GmbH, Weilheim, Germany). In the wet season, pH was measured with a Hach Lange pH meter (±0.005), and Chloride concentrations (Cl) measured by potentiometry were used to calculate salinity of the water samples (S = 1.806 Cl; Strickland & Parsons, 1968). For both instruments, conductivity and pH were calibrated with a 3 M KCL solution and NIST buffers (precision of 0.01%), respectively. Calibrations were performed before each survey.

DOC and δ^{13}DOC: Water samples were filtered on board under vacuum through 0.45 μm mesh size precombusted GF/F filters (Whatman microfiber, 25 mm diameter), acidified with 0.2 M HCl until pH 2, and stored at 4°C in 60 ml precombusted amber glass bottles.

Table 2
Depth-Wise Variations of Water Physicochemical Parameters in the Wet Season of 2015

Date	Time	Depth (m)	Temp (°C)	Salinity	Turbidity (NTU)	DO (% sat)	DO (μM)
09/06/2015	11:32–11:35	0.14 (0.00)	27.32 (0.07)	0.39 (0.46)	20.85 (3.52)	68.45 (1.36)	169.06 (3.12)
	11:37–11:41	1.17 (0.04)	27.15 (0.05)	13.99 (1.48)	27.20 (0.78)	58.36 (0.42)	134.04 (1.87)
	11:42–11:47	2.08 (0.02)	27.82 (0.00)	30.08 (0.06)	63.38 (5.87)	59.40 (0.07)	123.12 (0.31)

Note. Average values are shown and parentheses stand for standard deviations. High tide at 10:05.

CDOM, TA, and δ^{13}DIC: CDOM samples were filtered through 0.2 μm polycarbonate membranes (Whatman Nuclepore, 47 mm diameter) and stored in amber glass bottles and kept inside freezer on board. Filtrate was subsampled to store TA and δ^{13}DIC samples in 25 ml glass vials overfilled and screwed without any bubble formation.

Photosynthetic pigments (Chl-a and Pheophytin): 150 ml of water was filtered through 47 mm diameter 0.7 μm Whatman GF/F filters, and the residue was kept stored in freezer on board, then in dry ice during transportation, and finally in freezer at the lab until analysis.

TSM and POC/PN: Samples for TSM were stored in a cooler after filtration of 200 ml water on 47 mm Whatman GF/F filters; the latter were subsequently oven dried at 50°C for 24 hr and weighed. Elemental and isotopic samples of POC and PN were collected using preweighed and precombusted (overnight at 450°C) 25 mm Whatman GF/F filters (0. 45 μm mesh size), stored in the freezer in field, and subsequently freeze dried in the laboratory.

2.4. Laboratory Analyses

DOC concentrations (μM) were measured by High Temperature Combustion Oxidation (HTCO, Shimadzu TOC-VCSH). Acidified water samples after sparging with oxygen were injected onto a combustion column packed with platinum-coated alumina beads at 680°C. Nonpurgeable OC compounds were combusted and converted to CO_2, which was detected by a nondispersive infrared detector (NDIR). Calibration curves were computed using potassium hydrogen phthalate solution (KHP) ranging from 10 to 400 μM (coefficient of variation, CV < 2%). The δ^{13}DOC was analyzed by a HPLC system coupled to a Delta$^+$ XP IRMS through a LC IsoLink interface (Thermo Fisher Scientific, Germany; for instrumentation details, refer to Scheibe et al., 2012). The δ^{13}DOC values were reported as per mil relative to the PDB standard with an overall uncertainty of ±0.10‰. CDOM absorption spectra were measured following the NASA protocol (Mitchell et al., 2002) every nanometer from 250 to 850 nm using a double-beam Ultraviolet-Visible spectrophotometer (Shimadzu UV-2450; relative uncertainty within 0.02 to 0.03 m^{-1}).

TA was measured by gran titration (Automatic Potentiometric Titrator) with 0.1 N HCl with accuracy better than 10 μM. Alkalinity was also measured using a 96-well plate method adapted from Sarazin et al. (1999) and optimized for the analytical range 0–3 meq L^{-1}. DIC and $pCO_{2(water)}$ were calculated using CO_2SYS (Lewis & Wallace, 1998), with the carbonate dissociation constants K1 and K2 from Hansson (1973) refitted by Dickson and Millero (1987), and pH measured on the NBS scale. For the analysis of δ^{13}DIC, a headspace (<2 ml) was created, and H_3PO_4 was added to convert all DIC to CO_2. After overnight equilibration, part of the headspace was injected in the carrier gas stream of an elemental analyzer isotope ratio mass spectrometer (EA-IRMS: ThermoFinnigan Flash HT and ThermoFinnigan DeltaV Advantage) for δ^{13}C measurement. The δ^{13}DIC samples were collected and analyzed only for the dry season, because true observation of tidal time series trend was not achieved in the wet season (discussed subsequently) leading us to prioritize samples to be analyzed in foreign laboratory (KU-Leuven, Belgium).

Pigments (Chl-a and Pheo) were extracted for approximately 12 hr in 10 ml of 90% acetone at 4°C and analyzed with a Turner AU-10 Fluorometer. Chl-a extracts were acidified with 1 N HCl for pheophytin measurements, while Chl-a/Pheo ratio gave an index of the degradation state of the Chl-a.

POC and PN were analyzed by a Flash EA2000 (Thermo Fisher Scientific, Milan, Italy) consisting of a GC column and ECD detector. Relative uncertainties in the measurement of C and N were ±0.1 and ±0.03%, respectively. The δ^{13}POC was measured by a Thermo Finningan Delta plus mass spectrometer coupled with a Flash EA2000 and ConFloIV interface. All isotopic data are expressed in conventional delta (δ) notation, where the isotopic ratio (R) of $^{13}C/^{12}C$ is expressed relative to the international PDB standard as defined by δ value [‰] = $[(R_{sample}/R_{standard}) - 1] \times 1{,}000$. Relative uncertainties in the measurement of δ^{13}C and δ^{15}N were ±0.2 and 0.04%, respectively.

2.5. Estimating Air-Water CO_2 Flux

The CO_2 fluxes across the air-water interface were computed according to

$$F = k\,\alpha\,(p\mathrm{CO}_{2\mathrm{water}} - p\mathrm{CO}_{2\mathrm{air}}), \quad (1)$$

where F is the air-water CO_2 flux values (mmol m^{-2} day^{-1}), k is the gas transfer velocity or piston velocity (m day^{-1}), α (Bunsen coefficient, mol m^{-3} atm^{-1}; Wanninkhof, 1992) is the temperature- and salinity-dependent solubility of CO_2 (Weiss, 1974), and pCO_{2water} and pCO_{2air} are the partial pressures of CO_2 (μatm) in surface water and overlying air, respectively. Partial pressure is sometimes expressed as a fugacity considering nonideal behavior of CO_2 gas (Weiss, 1974), but because both partial pressure difference (ΔpCO_2) and fugacity difference (ΔfCO_2) have virtually the same numeric value, ΔpCO_2 was used. In the above equation, k normalized to a Schmidt number of 600 was computed as a function of wind speed (m s^{-1}), water current (cm s^{-1}), and water depth (m). There are several parameterizations of k developed for the oceans and estuaries (A. Borges et al., 2004; Raymond & Cole, 2001; Wanninkhof, 1992). In this study, piston velocity was calculated following k parameterizations developed for the mangrove dominated estuaries by Ho et al. (2016) in Shark estuary, Everglades, and Rosentrater et al. (2017) in tropical estuaries of the north-eastern coast of Queensland, Australia. The k was computed applying wind speed, water current, and bottom turbulence-induced formulae determined from dual tracer measurements ($k_{600} = 0.77\ v^{0.5}\ h^{-0.5} + 0.266\ u^2$; v = water current, u = wind speed, h = water depth) by Ho et al. (2016), and from floating chamber deployments ($k_{600} = -0.08 + 0.26\ v + 0.83\ u + 0.59\ h$) by Rosentrater et al. (2017). A positive F value denotes flux from the water to the atmosphere and vice versa.

2.6. Estimating Mangrove-Derived DOC, POC, and DIC

To quantify the amount of dissolved or particulate carbon added to or subtracted from the coastal water, a simple two component mixing model was applied (modified from Officer, 1976, and Mook & Tan, 1991).

$$C_{pred} = fC_R + (1-f)C_M \quad (1)$$

$$\delta^{13}C_{pred} = \frac{\left(C_R\delta^{13}C_R - C_M\delta^{13}C_M\right)S + \left(S_RC_M\delta^{13}C_M - S_MC_R\delta^{13}C_R\right)}{(C_R - C_M)S + (S_RC_M - S_MC_R)} \quad (2)$$

where f represents the salinity (S) fraction ($f = 1 - S/35$) and C_R and C_M are the fixed riverine and marine endmember concentrations, $\delta^{13}C_R$ and $\delta^{13}C_M$ are the riverine and marine endmember isotopic compositions, and S_R and S_M are the salinities of the two endmember, respectively. C_{pred} and $\delta^{13}C_{pred}$ denote predicted C and $\delta\ ^{13}C$ due to their conservative mixing. Such endmember mixing models of DOC, POC, and DIC (units in μM) and their isotopes along the salinity gradient (0 to 35) were previously applied for the Sinnamary estuary to compare observed data and values predicted by conservative mixing (see Ray, Michaud, et al., 2018).

The salinity values recorded during the 24-hr time series during the dry season were used in the above equations to compute predicted values of concentrations and isotopes of DOC, POC, and DIC. The lack of salinity variations (>70% of data representing freshwater) during the 12-hr survey in the wet season precluded using this data set for estimating mangrove-derived carbon. For the particulate fraction, our previous findings showed the consistent presence of lighter POC and stable salinity-wise distribution pattern (except steep POC decrease within 0–5 salinity) without much impact due to resuspension or deposition of the suspended matter at higher salinities (Ray, Michaud, et al., 2018), allowing us to estimate POC_{pred} from conservative mixing equations for the diel cycle.

Dry season-measured concentration and stable isotope endmembers (μM, ‰) used for the calculations were DOC (770, −29.5), DIC (195.8, −19.6) and POC (59.71, −39.41) for C_R and $\delta^{13}C_R$, and DOC (112, −23.1), DIC (2155.7, −5), and POC (24.9, −30.4) for C_M and $\delta^{13}C_M$. Salinity measured for riverine and marine endmembers was 0 and 35, respectively. A very prominent salinity gradient was observed within a short transect from the Sinnamary mouth to offshore during the dry season (see Ray, Michaud, et al., 2018). Hence, water flow from the river endmember allowed to carry nonmarine sources, such as mud bank derived from the Amazon basin and/or mangrove-derived products to offshore. For the marine endmember, this would explain the negative δ^{13}DIC value (−5‰ vs. ~ 0‰ for seawater usually) and the light δ^{13}POC value (−30‰ vs. approximately −22‰).

Deviations of the observed from the predicted C values (ΔC) are or nonconservative residual C,

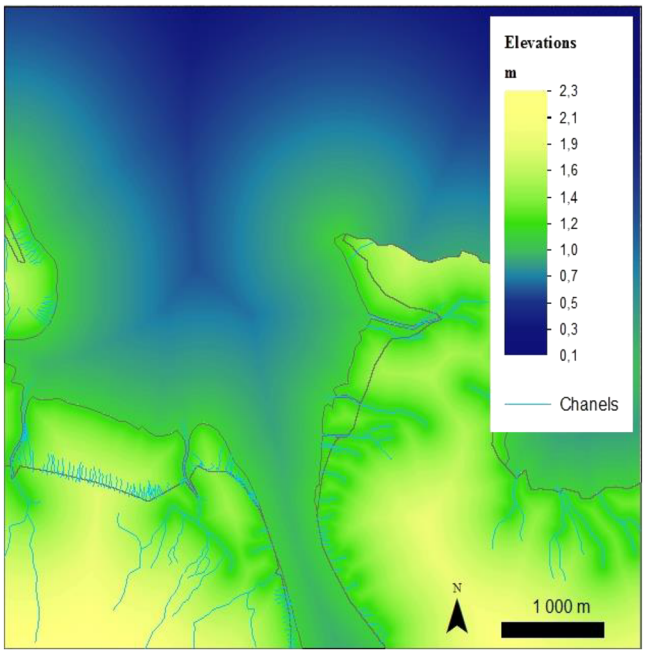

Figure 2. Mangroves and bare mud elevation levels in the Sinnamary estuary (French Guiana). The theoretical Digital Elevation Model (DEM) was constructed based on Euclidian distances and mean slope values using the water line observed on a Pleiades satellite image taken on 17 September 2015 at 14:13 UTC0 (1.65 m above the hydrographic reference; SHOM tidal model).

$$\Delta C = Cobs. - Cpred. \quad (3)$$

When, ΔC is positive, there is an "addition" of carbon into the estuary,

ΔC is negative, there is a "removal" of carbon from the estuary,

ΔC equals zero, there is "conservative" mixing of carbon in the estuary.

These estimates of ΔC can be used together with the mixing model and isotopic values of C, and the end-member C isotopic values, to estimate the isotopic value of the $\Delta^{13}C$ contribution at each measured data point. Therefore, the isotopic value of the nonconservative residual component ($\Delta^{13}C$) or the estimated $\delta^{13}C$ of excess C input for a given point along the salinity gradient can be estimated following Ray, Michaud, et al. (2018)

$$\Delta 13C = (Cobs.x\delta 13Cobs. - Cpred.x\delta 13Cpred.)/\Delta C. \quad (4)$$

Similar to ΔC, negative $\Delta^{13}C$ values suggest inputs of lighter carbon while positive values indicate inputs of heavier carbon. Using such a mixing model is meaningful only when C losses can be considered minimal and the concentrations are higher than expected from conservative mixing. Therefore, assuming that diagenetic reactions do not significantly alter the OM (Miyajima et al., 2009), positive ΔC in combination with negative $\Delta^{13}C$ at different time intervals would allow estimating the amount of carbon originating from the mangroves.

2.7. Mangrove-Driven C Exchange Flux by Digital Elevation Model

2.7.1. Modeling Elevations in the Study Area

A Digital Elevation Model (DEM; pixel ground size of 100 m^2) was used to quantify water fluxes and C exchange rates. As no DEM was available on public databases for this area and this period, we made a theoretical DEM using slope data from published literature and a high-resolution satellite Pleiades 2B image taken on 17 September 2015 at tide level 1.65 m above the hydrographic reference (Figure 2). The water line on the mud bank and in tidal channels was detected by photointerpretation of the satellite image in order to obtain a theoretical reference elevation line at 1.65 m height. Euclidian distances to this water line were then calculated from Spatial Analyst Toolbox for each 100 m^2 cell of a raster file covering the studied area. The distances were extracted below the water line (1), above the water line, and on bare mud (2) and, finally, above the water line and on mangrove coverage of age spanning 1 to 61 years (3) by using the "Extract by Mask" function. Polygons of mangrove ages were obtained as previously described in Ray, Michaud, et al. (2018). For areas situated below this water line, distances were multiplied by the mean slope (1:500) of bare mud surfaces published in Anthony et al. (2008) minus the water line elevation. For bare mud areas situated above the water line, the water line elevation was added to the product of distance and slope. For mangrove areas, the same methodology was employed using a mean slope (1:4,000) published by Proisy et al. (2009).

2.7.2. Calculating the Water Volume and Deriving C Fluxes

The water fluxes and associated C fluxes within the study area were estimated using our theoretical DEM, a SHOM tide model (uncertainties of ±5 cm in height and ±5 min in time) and equations of section 2.5. Fluxes of DOC, POC, and DIC, either exported from the mangroves or imported from the coastal waters, were calculated only for the dry season, when high-resolution sampling close to the mangroves was carried out, at high tide (at 10:30 and 21:40 on 18 November 2015) and low tide (at 15:30 and 4:20 on 18 and 19 November, respectively). Durations of the first and second tidal phases were 5 and 7 hr, respectively. Thus, total water volumes exchanged between the respective phases were calculated and averaged on hourly scale (water exchanges as Q1). Then, mangrove-derived carbon export or import rates (g C hr^{-1}) were calculated on hourly basis by multiplying ΔC of respective DOC, POC, and DIC in Equation 3 with Q1. Positive exchanges indicate C export flux while negative values denote import flux. Surface water carbon flux was further estimated per inundated surface area unit (g C m^{-2} day^{-1}).

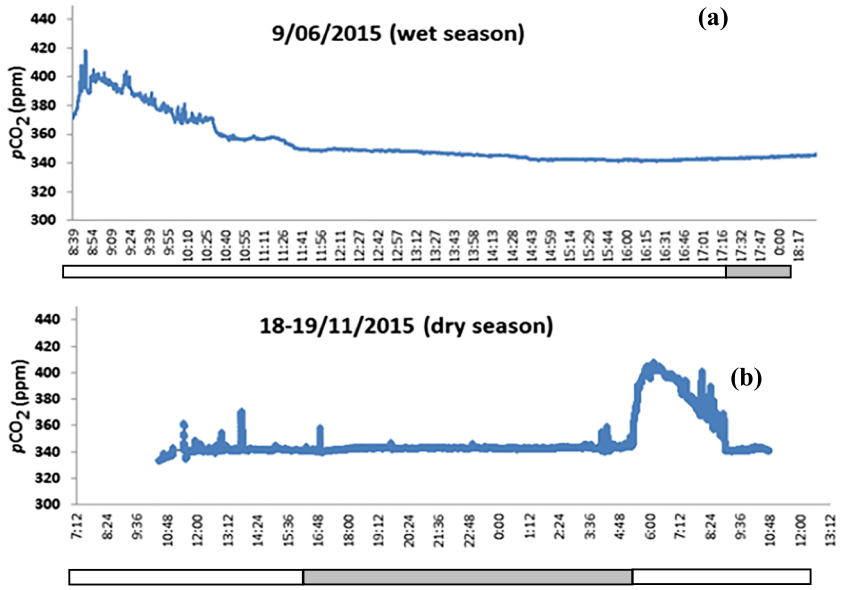

Figure 3. Atmospheric pCO_2 (ppm) recorded with a Li-COR (LI-820) in 12- and 24-hr time series surveys in the wet and dry seasons of 2015, respectively (see section 2.2). White and gray bar represents day and nighttime conditions, respectively.

Knowing river flow (Q2) at the downstream of the Sinnamary estuary in June and November 2015, estuarine exchange fluxes (F, in Mg C day^{-1}) of DOC, POC, and DIC to the adjacent Atlantic waters were calculated for both seasons by multiplying Q2 with the respective C concentrations at 0 salinity.

3. Results

3.1. Meteorological and Water-Column Environmental Parameters

3.1.1. The Wet Season

Atmospheric pCO_2 was higher in the wet season and exhibited a regular decrease during the morning, from 400–405 ppm at 9:00 to 345–350 ppm at 12:00 (Figure 3a). Most of the afternoon, values remained stable (344.7 ± 2.5 ppm from 12:00 to 18:30).

Site W located in the mainstream of the river channel mostly exhibited a freshwater signature in surface water in the wet season, even at high tide (salinity of 0.63 ± 0.60 from 8:20 to 11:34; Figure S1a in the supporting information). Marine bottom water was warmer, more turbid, and less oxygenated than surface water. Lowering of the YSI probe deployed from the boat from 11:42 to 18:56 (1.18 ± 0.39 m depth) showed that marine water was still present near bottom 2.5 hr after high tide (Figure S1b). Then, dilution by river water led to near-zero salinity in bottom water from mid-ebb to mid-flood of the tide. Water temperature exhibited little variations according to tide or depth (27.09 ± 0.43 and 27.25 ± 0.29°C in surface and bottom water, respectively). Mean surface water current varied from 0.2 to 1.13 m s^{-1}. Turbidity remained low during the survey (31.6 ± 5.7 and 87.8 ± 70.2 NTU in surface and bottom water, respectively), except for a bottom-w peak (297.3 ± 113.6 NTU) lasting for 35 min during the second half of the ebb. Mean DO concentration in surface and bottom waters in the wet season was 164.5 ± 3.7 μM (66.4 ± 1.2% saturation) and 154.2 ± 17.2 μM (63.8 ± 4.1% saturation), respectively. DO saturation mainly varied near bottom where it was minimum close to midebb (53%) before increasing with freshwater mixing (up to 67%). Stable conditions were then recorded during the end of the ebb and beginning of the flood. Mean Chl-a concentration recorded in surface/subsurface water (0.65 ± 0.23 m depth) during the 12-hr survey was 5.9 ± 6.4 μg L^{-1}, with peaks (33.5 ± 23.1 μg L^{-1}) observed close to midebb tide in surface water (data not shown). Stratification at mid-ebb ranged from Salinity 0 at 30-cm depth to 23.3 at 1.7-m depth (YSI probes data).

3.1.2. The Dry Season

Wind speed varied between 1.3 and 7.3 m s^{-1} in the dry season, with maximum and minimum values usually occurring during the day and at night, respectively. Atmospheric pCO_2 on 18 November was stable

throughout the day and most of the night (342.4 ± 2.2 ppm from 10:28 on 18 November to 5:20 on 19 November) but suddenly increased up to 403–407 ppm at sunrise (Figure 3b). Then, $pCO_{2(air)}$ started decreasing again from 6:30 on to reach 345–350 ppm at 9:00 (341.8 ± 0.8 ppm from 9:00 to 10:45).

Site D located close to the mangrove mud bank exhibited a marine signature in surface water during the late flood and early ebb (salinity of 33.87 ± 0.64; Figure S2a). Mean surface water salinity over the 24-hr time series (16.7 ± 12.17) was higher than during the wet season. Marine water was first detected during the flood near bottom, where it lasted for 8 hr (salinity > 33 from 17:40 to 1:40; Figure S2b). Thus, the marine influence was twice longer in bottom water, compared with surface water. Salinity at low tide was also higher in bottom water (6–12) compared with surface water (3–6). Water temperature showed little variations according to tide or depth (29.18 ± 0.45 and 29.4 ± 0.48°C in surface and bottom water, respectively) and was warmer of 1.6–2.1°C than during the wet season. Mean surface water current varied from 0.01 to 0.98 m s^{-1} (0.3 ± 0.2 m s^{-1}). Water turbidity was higher on average during the dry season (140.3 ± 137.3 NTU in bottom water), with main peaks (up to 800–1,000 NTU) occurring 2 to 3 hr after low tide (Figure S2b) together with DO decreases. Mean DO concentration in surface and bottom waters in the dry season was 150.3 ± 14.2 μM (68.8 ± 7.3% saturation) and 135.9 ± 15.4 μM (66.8 ± 8.4% saturation), respectively (Figure S2). DO concentration and saturation mainly varied with tide and followed salinity variations whatever the depth. Overall, the difference between surface and bottom water DO saturation was ~5% in both seasons. Mean surface-w Chl-a concentration during the 24-hr survey was 4.4 ± 2.3 μg L^{-1}, with peaks (8 to 27 μg L^{-1}) occurring at low tide—beginning of the flood—and high tide—beginning of the ebb.

3.2. Time Series of C Concentration, Isotopes, Absorption, and Fluxes

No clear pattern of salinity change with tide was observed in the wet season. By contrast, salinity varied accordingly with tidal height in the dry season except at 23.30 (18 November) and 00.30 (19 November) when abrupt drops of salinity down to 5 and 6.4 were recorded (Figure 4). Salinity as a conservative tracer is used as reference of water mass mixing that can explain modifications in temporal patterns of C pools.

3.2.1. DOC, δ^{13}DOC, and CDOM

No clear tidal pattern in DOC was observed in the time series, but DOC concentration varied between seasons/sites from 441 to 627 μM in the wet season ($n = 11$) and from 523 to 952 μM in the dry season ($n = 24$; Figure 4). The δ^{13}DOC displayed inverse tidal trend, ranging from −28.9‰ to −24.6‰ in the dry season ($n = 13$), with most depleted values observed at minimum salinities (S and δ^{13}C: 4.8‰ and −28.8‰; 4.7‰ and −28.9‰; 5.6‰ and −28.9‰, respectively) and most enriched values at higher salinities (S and δ^{13}C: 22.6‰ and −24.6‰; 20.3‰ and −25.9‰, respectively). Such pattern was not observed during the wet season (δ^{13}C ranging from −31.5‰ to −29.7‰, $n = 11$).

A clear tidal trend was observed in CDOM absorption coefficient ($a_{cdom}412$) in the dry season (Figure 4) with higher values at low tide (2.52 m^{-1} for $S = 4.7$) and lower values at high tide (0.48 m^{-1} for $S = 25.4$; $n = 24$). Slope at 275–295 nm ($S_{275–295}$) followed the same distribution pattern as salinity in the dry season, ranging from 0.014 to 0.016 nm^{-1} ($n = 24$). The ratio between CDOM and DOC (described as $a_{cdom}(412)$/DOC, hereafter a_{cdom}*(412)) mirrored the changes of $a_{cdom}412$, being maximum at low tide (3.95 m^2 mol^{-1} for $S = 5.4$) and minimum at high tide (0.67 m^2 mol^{-1} at $S = 25.4$). Time series of the CDOM descriptors in the wet season did not show any clear pattern either with salinity or tidal height.

3.2.2. TSM, POC, δ^{13}POC, and Chl-a

TSM mirrored tidal variations in the dry season (figure not shown), being highest at high tide and lowest at low tide (range 22–197 mg L^{-1}), whereas such trend was absent in the wet season (range 48–724 mg L^{-1}). POC concentration varied significantly between seasons (wet season: 70–352 μM, $n = 11$; dry season: 13–42 μM, $n = 24$; Figure 5). POC showed overall increase in concentration with increasing salinity and water height only in the dry season. Nearly reverse trend was observed for the POC:TSM ratio at that time (max: 1.14% for $S = 5.1$; min: 0.10% at $S = 16$). Elemental ratios of suspended matter (POC:PN) showed similar diurnal pattern as POC:TSM in the dry season, except one night (21:30) value for $S = 15.3$, where high POC concentration led to higher POC:PN ratio (12.2). The latter might be due to sediment resuspension, which is supported by high TSM content (93 mg L^{-1}). Lack of two TSM samples in the wet season precluded identifying any temporal trend between those ratios. No tidal variation was observed in Chl-a concentration in the wet season (hourly water samples: 1.6–4.2 μg L^{-1}) in contrast to the dry season (1.0–5.9 μg L^{-1}; max. at high tide and $S = 25.4$ vs. min. at low tide and $S = 5$). Similar observation was found for the Pheophytin

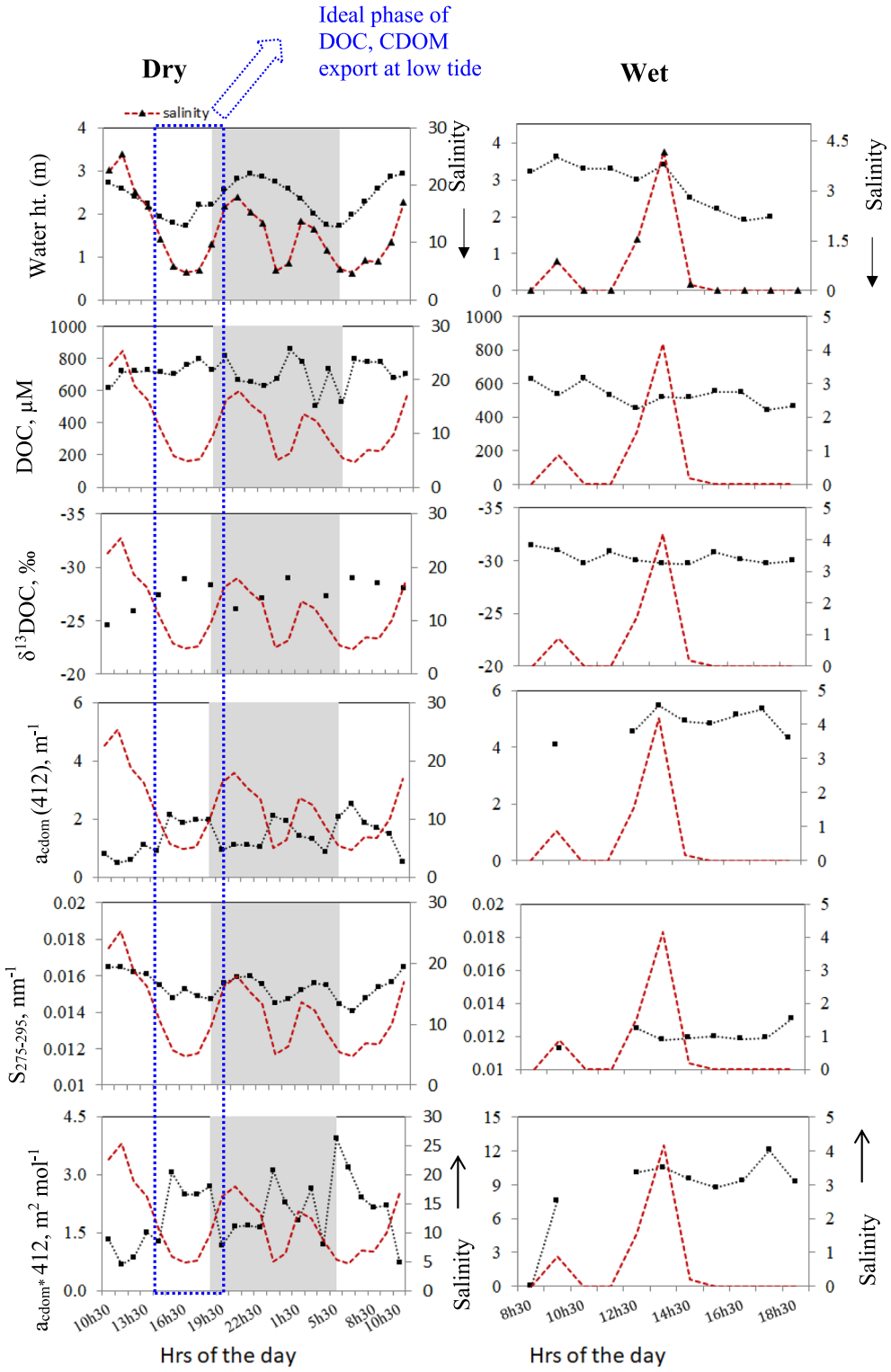

Figure 4. Tidal variations of surface water DOC (µM), δ^{13}DOC (‰), and CDOM parameters like the absorption coefficient at 412 nm ($a_{cdom}(412)$, m^{-1}), slope at 275–295 nm ($S_{275-295}$, nm^{-1}) and CDOM normalized to DOC (a_{cdom}*412, m^2 mol^{-1}) during the 24- and 12-hr surveys carried out in the dry and wet seasons of 2015, respectively. Tidal height (m) and salinity (red dashed line) are also represented on the figure. Vertical gray band representing the dark phase of the sampling period (18h30 to 5h30), and the blue box area describing the ebb tide period when mangrove-derived DOC and CDOM leaching was maximum as evidenced by stable isotope and optical indexes (refers to section. 4.3.1).

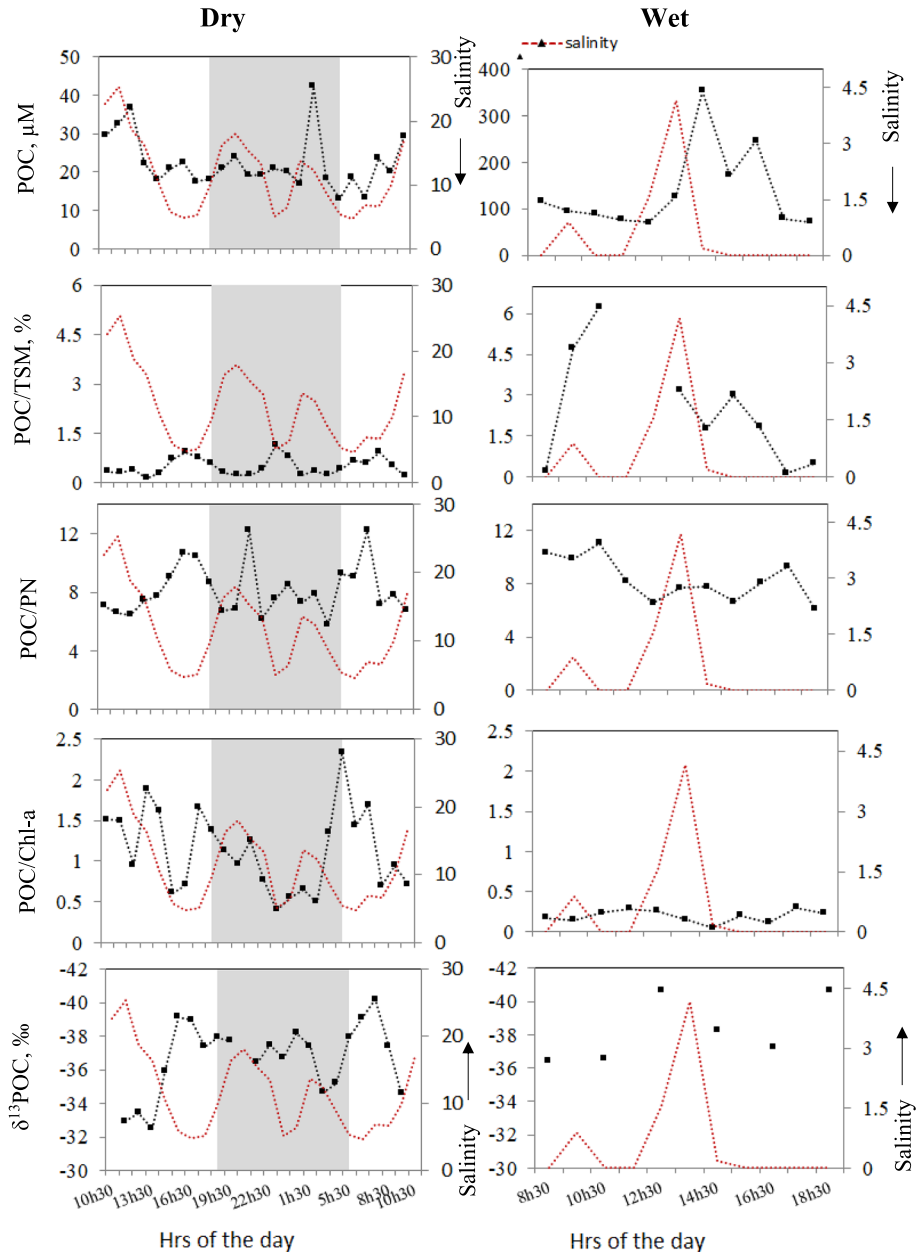

Figure 5. Tidal variations of surface water POC (µM), and relative contributions of POC to TSM (%), POC to PN (%), and POC to Chl-a (mass based), and δ^{13}C-POC (‰) during the 24- and 12-hr surveys carried out in the dry and wet seasons of 2015, respectively. Red dashed line: salinity. Vertical gray band representing the dark phase of the sampling period (18h30 to 5h30).

concentration, that is, no tidal trend in the wet season (1.2–4.3 µg L^{-1}) in contrast to the dry season (1.2–3.7 µg L^{-1}, max. at $S = 5.8$ and min. at $S = 10$; figure not shown).

The POC: Chl-a ratio (mass based) did not show any clear variation with salinity but varied seasonally (wet: 330–1,802, dry: 42–250).

In the dry season, extremely depleted δ^{13}POC values were measured at lower salinities (e.g., −39.13‰ for $S = 5.8$; −40.2‰ for $S = 6.9$) while the most enriched δ^{13}C value was measured at highest salinity (−32.9‰ for $S = 25.4$). No such trend was found in the wet season, when δ^{13}C varied from −40.66‰ to −36.45‰ for salinity in the range 0–4.2.

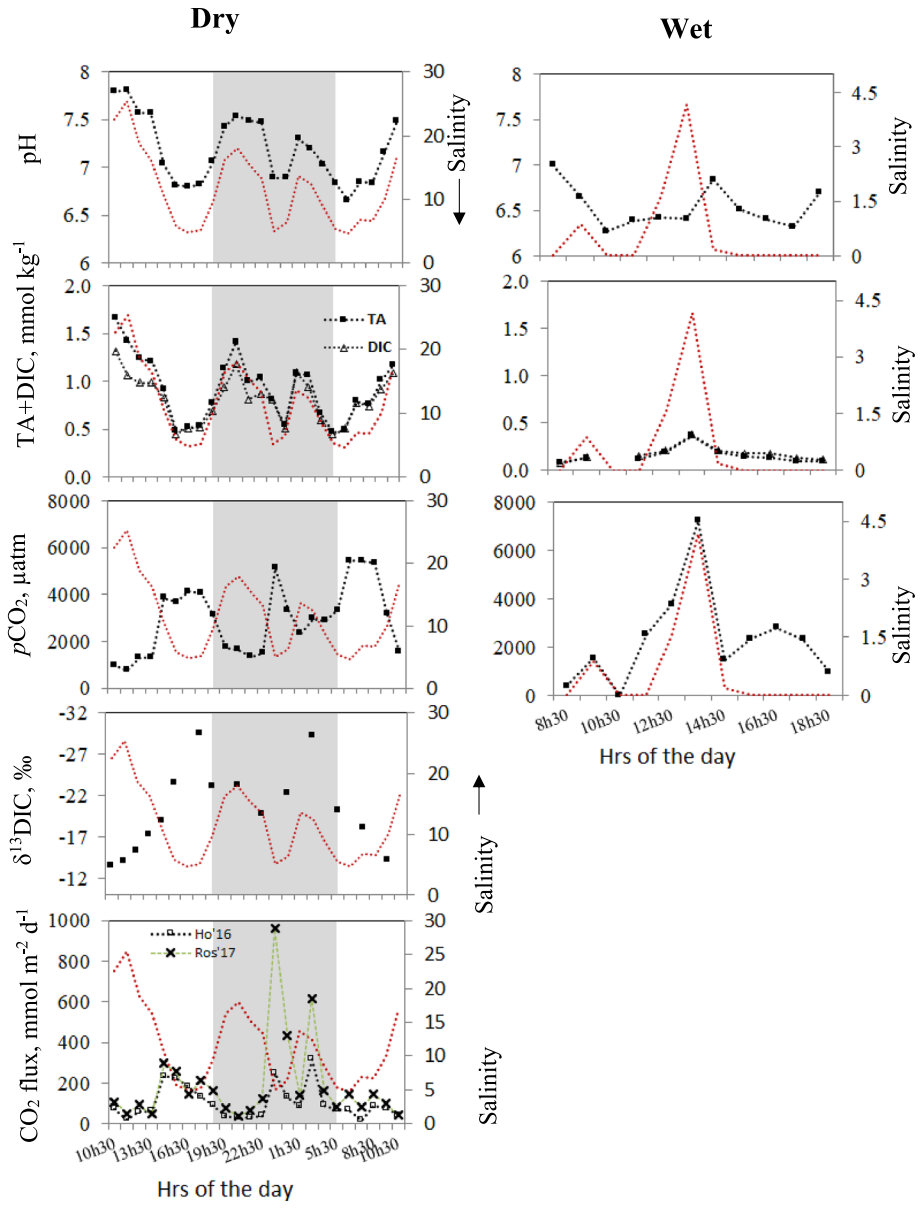

Figure 6. Tidal variations of surface water pH, total alkalinity (TA) plus DIC (mmol kg^{-1}), pCO_2 (µatm), δ^{13}C-DIC (‰), and air-water CO_2 exchange flux (mmol m^{-2} day^{-1}) during the 24- and 12-hr surveys carried out in the dry and wet seasons of 2015, respectively. The δ^{13}C-DIC and air-water CO_2 exchange fluxes calculated by the Ho et al. (2016) (as Ho'16) and Rosentrater et al. (2017) (as Ros'17) models are only shown for the 24-hr time series. Red dashed line: salinity. Vertical gray band representing the dark phase of the sampling period (18h30 to 5h30).

3.2.3. DIC and Air-Water CO_2 Flux

Tidal trend of pH was unclear in the wet season while pH followed diel salinity variability in the dry season, being highest (7.80) at high tide and lowest (6.66) at low tide (Figure 6). TA and DIC concentrations remained <0.4 mmol kg^{-1} during the wet season. Tidal trends of TA and DIC concentrations were similar to pH, ranging from 0.47 to 1.66 mmol kg^{-1} and 0.44 to 1.32 mmol kg^{-1}, respectively ($n = 24$). Surface water pCO_2 values were well above atmospheric equilibrium along the entire salinity range during both time series. In the wet period, $pCO_{2(water)}$ (391–7,216 µatm, $n = 10$) did not show clear tidal trend due to low salinity variations, while opposite trend was found between $pCO_{2(water)}$ (1,360–5,461 µatm) and salinity in the dry period. Sharp depletion pattern of δ^{13}DIC was observed during the day in the dry season (no data in wet

season), δ^{13}DIC being maximum at 10:30 at high tide (−13.57‰) and minimum at 17:30 at low tide (−29.45‰; $n = 15$). The more depleted δ^{13}DIC values (−19.83‰ to −29.23‰) were generally observed during the night.

Air-water CO_2 flux (F) in the dry season varied with tide overall, with minimum values observed at higher salinities and vice versa (Figure 6). Fluxes were always positive in both Ho et al. (2016) and Rosentrater et al. (2017) models (102 ± 81 and 191 ± 211 mmol m^{-2} day^{-1}, respectively), while differences in hourly piston velocity (11 ± 7 and 6.3 ± 3.5 cm hr^{-1}, respectively; data not shown) explained flux variability between the two calculations. High uncertainty (CV > 100%) in mean F_{CO2} calculated by Rosentrater et al. (2017) was due to the outlier observed at 23:30 (960 mmol m^{-2} day^{-1}); if we discard this unlikely value (much greater than the global average for mangroves: 60 ± 45 mmol m^{-2} day^{-1}; Bouillon et al., 2008), the revised F_{CO2} would be 157 ± 136 mmol m^{-2} day^{-1}.

3.3. Exchanges of DOC, POC, and DIC Between Coastal and Mangrove Systems

DOC concentrations measured during the dry season were higher than predicted values (except two points; Figure 7) resulting in 91% positive values of residual DOC (ΔDOC). By contrast, POC produced 100% negative values of residual POC (ΔPOC). DIC did not follow a clear pattern: Positive and negative values of residual DIC (ΔDIC) were in equal proportion (~54% positive), indicating both addition and removal were regulating surface water DIC concentrations. Similarly, 50% negative and positive values were obtained for residual isotopic DIC (Δ^{13}DIC) versus 100% negative values for DOC (Δ^{13}DOC) and POC (Δ^{13}POC) (Figure 8).

Using the DEM and tidal model, it is estimated that total water flows (Q1) for the first and second tidal phases were about 614 and 528.6 m^3 s^{-1}, respectively, averaging Q1 to 571.4 ± 60 m^3 s^{-1} for a complete tidal cycle on 18 November 2015. Hourly fluxes of DOC, POC, and DIC are shown in Figure 9. DOC made the largest contribution to carbon export from the Sinnamary mangroves, ranging from 0.32 to 10.3 Mg C hr^{-1} (1 Mg = 10^6 g) except two negative (import) values. POC was imported to the mangrove throughout the tidal cycle (−0.05 to −1.02 Mg C hr^{-1}) with the largest rates occurring at low tide. DIC was either exported or imported according to tide, ranging from −12.8 to 10.13 Mg C hr^{-1}, with no clear tidal pattern especially during the night. DIC export from the mangroves was mainly observed at night. Net fluxes of DOC, POC, and DIC for a neap tide cycle of the dry season were 92.3, −15.3, and −10.2 Mg C day^{-1}, respectively. Since total area of inundation in the Sinnamary mangrove was estimated to be 1,134 ha, DOC, POC, and DIC export or import fluxes per inundated surface area unit were estimated to be 8.14, −1.35, and −0.90 g C m^{-2} day^{-1}, respectively. Summary of these results and their derivations are shown in Table 3.

3.4. Riverine Exports of DOC, POC, and DIC to the Atlantic Ocean

In the wet season, the sampling site located along the river channel (W) exhibited minor salinity deviations from 0 throughout the 12-hr time series. Thus, C concentrations at Site R (DOC = 604 μM, POC = 101 μM, DIC = 110 μM; Table 3) were averaged with the C values at Site W to estimate mean estuarine concentrations of DOC (550 ± 70 μM), POC (119 ± 61 μM), and DIC (143 ± 43 μM) at Salinity 0.

In the dry season, DOC, POC, and DIC concentrations at Site R were 692 ± 100, 75 ± 22, and 143 ± 105 μM, respectively (Table 3). Since there was no freshwater endmember recorded at Site D, we took C values from Site R to estimate riverine exports. The Sinnamary downstream riverine exports of surface water DOC, POC, and DIC to the adjacent Atlantic coastal waters were calculated to be 285–399, 61–86, and 74–104 Mg C day^{-1}, respectively, for the wet season and 118–158, 11–19, and 8–49 Mg C day^{-1}, respectively, for the dry season (min. − max. values).

4. Discussion

4.1. Study Limitations and Hydrological Features

The lack of salinity gradient and marine endmembers in the wet season sampling did not favor comparison of the biogeochemical data sets between seasons. A very weak salinity-property relationship was observed for the wet season, while tidal and mangrove influences could be traced in the dry season. Indeed, surface water salinity at Station W (wet season) did not vary with the tide (close to 0), when it showed normal tidal pattern at Station D (dry season), increasing with the flood (up to 25) and decreasing with the ebb (down to

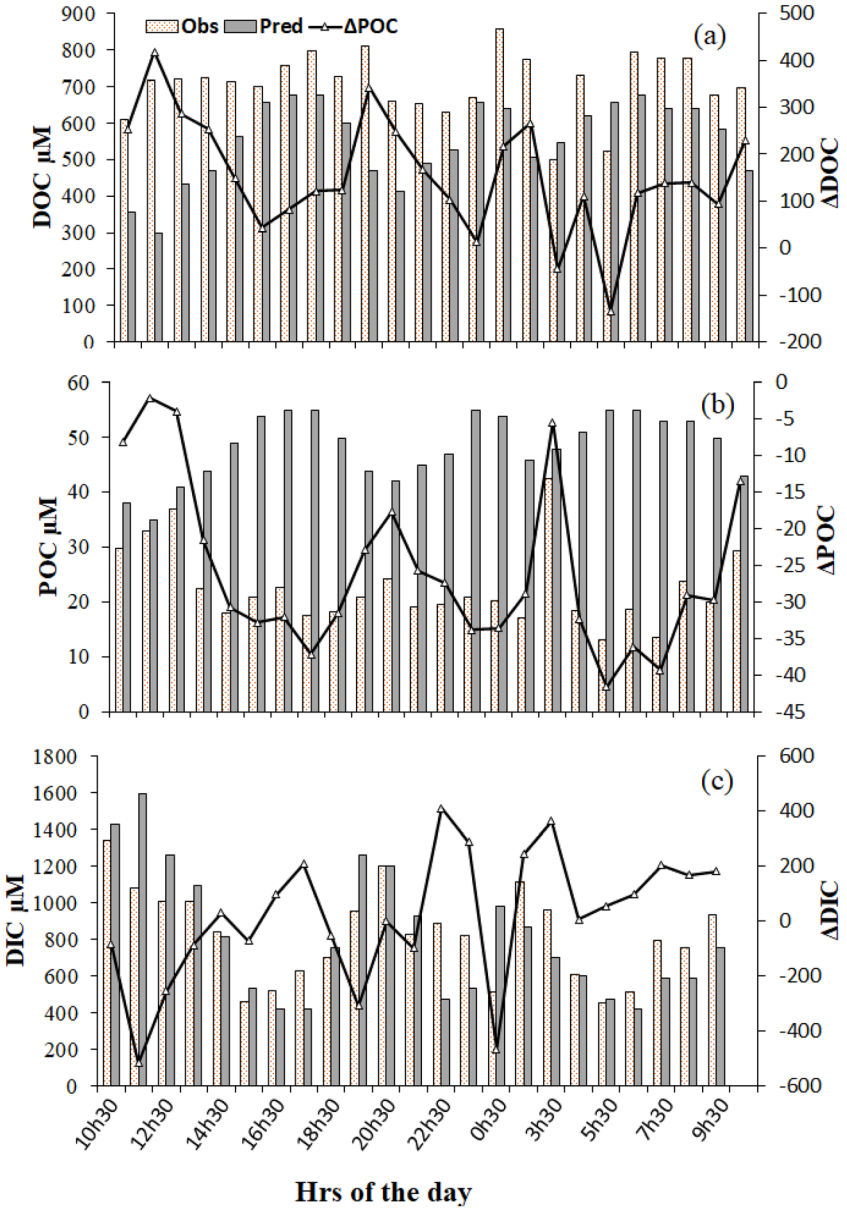

Figure 7. DOC, POC, and DIC (µM) "internally added" to the estuary (mangrove-derived) during the 24-hr time series in the dry season of 2015. ΔC is defined as nonconservative residual C.

5). Different geographic location of the sampling stations would partly explain such pattern: Station W was located right across the river channel whereas Station D was closer to the mangrove-seashore transition (Figure 1) and influenced by the marine and river water mixing. Hourly monitoring by WTW probe during water sampling did record salinity increases at 1:30 and 3:30 (ebb tide) on 19 November (Figure 4), which would be indicative of a gyre circulation close to the mud bank edge. Higher freshwater inputs sustained by greater rainfalls and river discharge in the wet season would also explain seasonal variations. YSI deployments at different depths showed that the halocline was more pronounced in the wet season than in the dry season (Table 2 and Figures S1 and S2). Freshwater discharge spread over the denser sea water, thus allowing superposition of both water masses in the area. If annual rainfall in FG in 2015 was similar (+1%) to the 30-year average value (1981–2010) calculated by Météo France (https://donneespubliques.meteofrance.fr/donnees_libres/bulletins/BCA/BCA_973_2015.pdf), the main rainy season (April–June) was shorter (10 May to 15 June) but more pronounced (+4%) than the 30-year trend, while the 2015

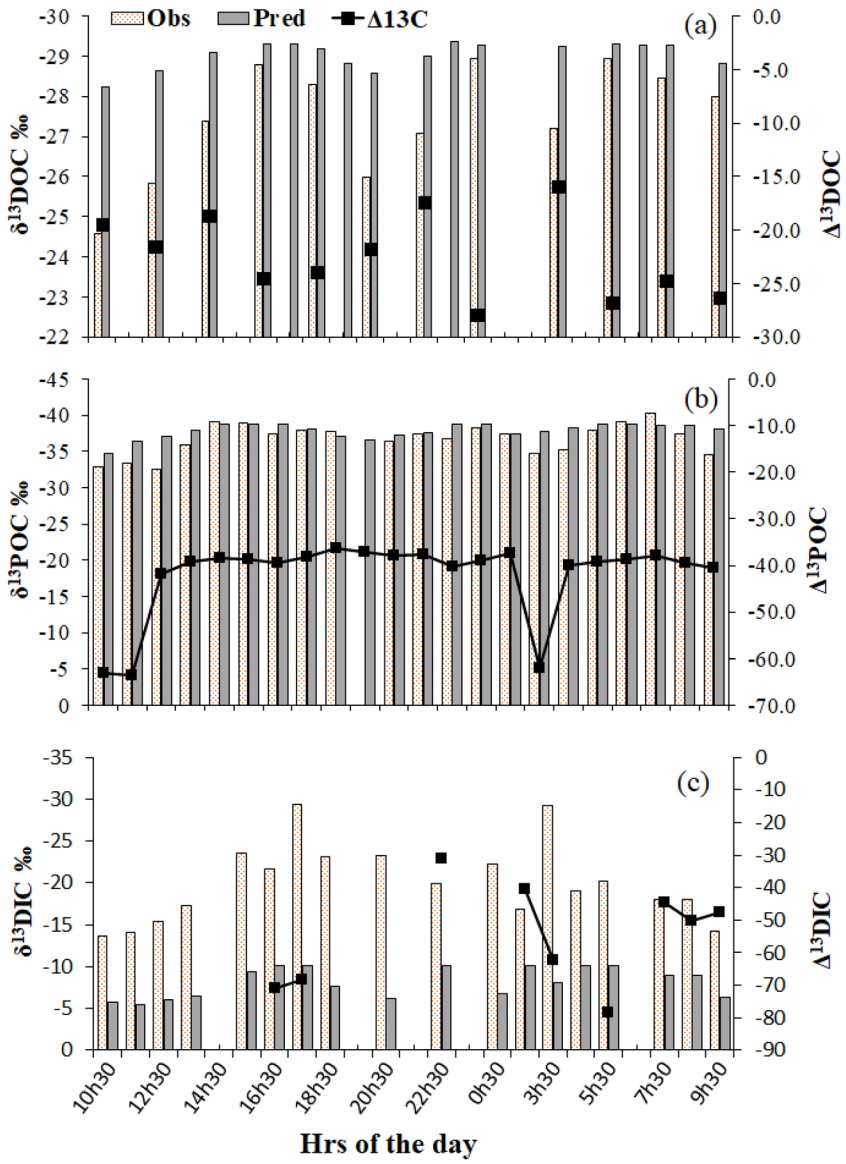

Figure 8. $\delta^{13}C$ values (‰) of DOC, POC, and DIC "internally added" to the estuary (mangrove-derived) during the 24-hr time series in the dry season of 2015. Few unusually high $\Delta^{13}C$-DIC are not shown, and only consistent values are given and described in the text.

ENSO event led to a major rainfall deficit (−23%) during the dry season (including November). Hence, mangrove-derived flux estimates of DOC, POC, and DIC are expected to increase in the wet season due to higher freshwater drainage.

The lack of meteorological parameters in the wet season did not allow calculating air-water CO_2 exchange flux at that time and precluded estimating seasonal variability of this flux. We also expect significant variations of CO_2 flux according to tide (spring vs. neap tides) and at spatial scale (linked to distance from the mangroves). In particular, tidal flow patterns at both neap and spring tide should be measured for the study of C fluxes. Higher mangrove surface area immersed, longer immersion time and high water current during spring tides could enhance the input of particulate organic matter originating from the mangrove end that otherwise might be restricted at neap due to less benthic inundation and low water current (Hemminga et al., 1994). Conversely, microbial-mediated DOC decomposition rate was found higher at neap tide (1.2–4.7 $\mu M\ hr^{-1}$) than at spring tide (0.5–1.4 $\mu M\ hr^{-1}$), favoring more DIC production and DOC consumption at neap (refer to the results in SE Asian mangroves by Kristensen & Suraswadi, 2002). Therefore, it is

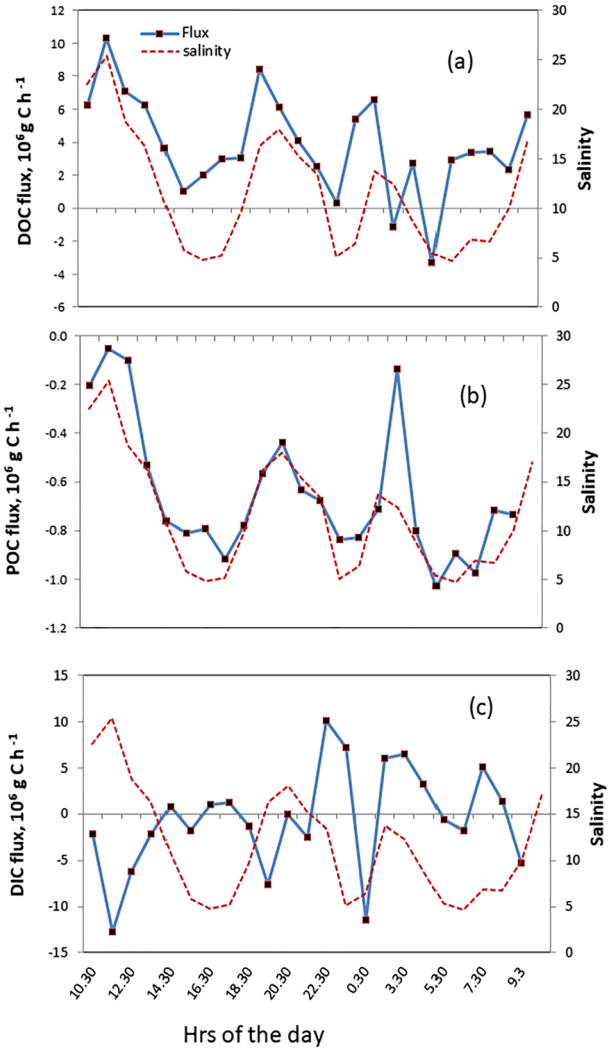

Figure 9. Hourly fluxes of DOC, POC, and DIC (10^6 g C hr^{-1}) in surface water during the 24-hr time series in the dry season of 2015. Negative fluxes indicate C import, and positive fluxes indicate C export.

necessary to capture C concentration and fluxes in both tidal conditions, which is a limitation of the present study.

4.2. Atmospheric Features During the Study Period

Overall low atmospheric pCO_2 mixing ratios were recorded during this study; in addition, unexpected variations were observed during the 24-hr survey in November 2015, which are very stable values (342 ppm) during the day of 18 November and following night, but a sudden increase on 19 November from 5h30 on (up to 408 ppm), which maintained until ~8h20, and a decrease in pCO_2 to return to the previous value of 342 ppm from 9h00 onward. We first looked at the wind and pCO_2 data from the canopy of the primary rain forest at Paracou (Guyaflux site, 53.0′W 5.2′N) to see how the CO_2 exchanges at the canopy could impact the Sinnamary estuary and mangroves depending on the wind regime. In fact, this influence would be minor due to the dominant Alizées winds blowing from NE to SE in this region (90% to 95% of annual data; Damien Bonal, CIRAD Kourou, personal communication in July 2017) and the coastline orientation (NE). The wind data recorded by the LEEISA meteorological station in November 2015 confirmed this pattern: A NE-ENE wind was blowing on 18 November and following night until 5h20, when the wind turned to SE-SSE. This latter inland wind maintained until 9h00, and then wind returned to NE-ENE. Indeed, we recorded the ocean signal most of the time during the 24-hr survey in November 2015. Now, Buchmann et al. (1997), who measured pCO_2 in the canopy of the rain forest at Paracou in late September 1994 and mid-July 1995, used the tropospheric pCO_2 values measured at Barbados as the ocean signal (baseline concentrations). Monthly mean values recorded in September 1994 (dry season) and July 1995 (wet season) were 353.7 and 360.4 ppm, respectively. Our "mean ocean" values recorded in 2015 during the dry and wet seasons were slightly lower than these values (342 and 345 ppm, respectively) and could reflect the role of the oceanic carbon pump. At higher salinities in the dry season, Ray, Michaud, et al. (2018) observed typical "marine DIC" signal (~2.0 mmol kg^{-1}, δ^{13}DIC ~ −5.5‰) pointing to the DIC uptake by marine phytoplankton. Similarly, offshore pCO_2 concentrations were twofold to threefold more depleted than the

Table 3
Summary of the Seasonal C Concentrations and Estuarine and Riverine Fluxes

Dry season Site D	Observed conc. (μM) C_1	Conservative conc. (μM) C_2	Residual conc. (μM) $\Delta C = (C_1 - C_2)$	Tidal water flow (m^3 s^{-1}) Q_1	Inundated area (10^4 m^2) A	Estuarine C exchange/h (mg C hr^{-1}) $\Delta C \times Q_1 \times cf_1$[a]	Estuarine C exchange rate (g C m^{-2} day^{-1}) $\Delta C \times Q_1 \times A$
DOC	708 ± 84	552 ± 109	156 ± 122	571.4 ± 60	1,134	3.8 ± 3.0	8.14
POC	22 ± 7	48 ± 6	− 26 ± 11	571.4 ± 60	1,134	− 0.6 ± 0.3	−1.35
DIC	822 ± 246	812 ± 349	18 ± 241	571.4 ± 60	1,134	0.4 ± 5.9	−0.90

Dry season Site R	Observed conc. (μM) C_3	River water flow (m^3 s^{-1}) Q_2	Riverine export (Mg C day^{-1}) $C_3 \times Q_2 \times cf_2$[b]	Wet season Site R & W	Observed conc. (μM) C_4	River water flow (m^3 s^{-1}) Q_3	Riverine export (Mg C day^{-1}) $C_4 \times Q_3 \times cf_2$
DOC	692 ± 100	193	118–158	DOC	550 ± 70	700	285–399
POC	75 ± 22	193	11–19	POC	119 ± 61	700	61–86
DIC	143 ± 105	193	8–49	DIC	143 ± 43	700	74–104

Note. The table includes formulas used to calculate fluxes from observed concentration (C_n), water discharge (Q_n), and inundated area (A) values. Results are given as mean ± SD and ranges (where applicable). Estuarine C exchange rate equals to the rate of "mangrove-derived C" (see Table 4).
[a]cf_1 = first conversion factor = 43.2×10^{-6}. [b]cf_2 = second conversion factor = 1036.8×10^{-6}.

inshore waters due to oceanic primary production. The November 2015 pCO_2 values were similar to the November 2013 values (332–340 ppm) recorded on the pioneer mangrove. However, these low concentrations question the average increase in atmospheric pCO_2 between the years 1994–1995 and today for the oceanic signal (e.g., see Takahashi et al., 2009).

4.3. Tidal Variations and Sources of DOC, POC, and DIC

4.3.1. Dissolved Organic Carbon

The best period for DOC and POC exports from mangroves to adjacent estuarine waters would be the early ebb tide (de Rezende et al., 2007) when carbon is flushed out of the system via litter leaching (decaying leaves as OC source) and porewater drainage. In our study, only DOC was exported during the dry season. Surface water DOC levels consistently increased (30% to 50%) with decreasing salinity (ebb tide), due to more sedimentary organic matter leaching. Isotopic composition emphasized prominent mangrove signature for DOC at low tide (mean: −29‰), when compared with $\delta^{13}C$ values of *Avicennia* litter and leaf (−30.5‰; this study), mixed microphytobenthos (−20.9‰; Ray, Michaud, et al., 2018), and marine phytoplankton (−22‰; Cifuentes et al., 1996). Tidally mediated sediment-water exchanges and porewater drainage are known vectors for DOC exchanges with estuarine waters or mangroves (Schwendenmann & Veldkamp, 2006). The formers have a stronger effect on the biogeochemical cycling in the estuary than the fluvial inputs during a dry compared to a wet season (Mori et al., 2019). In French Guiana, threefold to fourfold higher DOC concentration in porewater than in tidal water provides reasonable evidence of export of litter-sourced DOC during the ebb (Ray, Michaud, et al., 2018). DOC enrichment in estuarine water at low tide has been observed in other mangroves (Bouillon et al., 2007; Dittmar & Lara, 2001; Maher et al., 2013; Ray, Baum, et al., 2018; Twilley, 1985). Marine-imported DOC with typical $\delta^{13}C$ value of −22‰ mixed with mangrove-derived DOC and ultimately enriched δ^{13}DOC during the rising tide.

The Sinnamary estuary acted as a perennial source of DOC as evidenced by the positive nonconservative DOC component (ΔC) in the 24-hr time series (Figure 7a) and net daily addition of 155 ± 122 μM DOC with $\Delta^{13}C$ of −22.4‰. Distinctive changes in residual $\Delta^{13}C$ with tide suggested a tidal control over DOC sources (Figure 8a). Dominance of mangrove leaf/litter signature in the DOC pool was quite prominent at low salinities ($\Delta^{13}C = -27.89$‰ to −24.52‰ for $S \sim 5$) versus marine phytoplankton and/or microphytobenthos signature at higher salinities ($\Delta^{13}C = -21.55$‰ to −19.44‰ for $S = 19$–22). Unusually heavy Δ^{13}C-DOC of approximately −16‰ at Salinity 8.7 might be indicative of bottom water originated pure benthic algae, which would agree with the YSI probe data (peaks of bottom-w turbidity and surface-w Chl-a; Figure S2).

Similar to the tidal trend of DOC, CDOM absorption exhibited a 4 to 4.5-fold increase from high tide to low tide reflecting the export of optically active DOM from the mangroves during the ebb. CDOM slope at 275–295 nm, a proxy for terrigenous DOM, decreased during ebb tide highlighting the presence of high molecular weight litter sourced DOM, in line with depleted δ^{13}DOC. Like other plants, mangrove leaves contain substantial optically active tannin components (Forest et al., 2004; Hernes et al., 2001). Highly colored DOC pool at low tide (assigned by DOC-specific CDOM absorption or a_{cdom}*412) pointed out persisting tannin compounds leached from the litter. Tannins are replaced by low molecular weight, less colored DOC derived from marine sources during the flood. Similar tidally driven CDOM fluctuations were found in other mangroves, sea grasses, and marshes, where sources such as litter, floating macrophytes, protein-like compounds released from phytoplankton cell lysis, and benthic decomposition of microphytobenthos would change the DOM optical properties (Cawley et al., 2013; Romera-Castillo et al., 2010; Shank et al., 2010; Watanabe & Kuwae, 2015).

4.3.2. Particulate Organic Carbon

Tidal variations of POC in the dry season were controlled by both marine import and mangrove export. On one hand, high POC:TSM ratio and low POC:PN ratio (6.5–7.8) at high tide could be attributed to marine phytoplankton and resuspended microphytobenthos (MPB), though the trend for the POC:Chl-a ratio was unclear. On another hand, the threefold increase of the relative proportion of POC to the TSM pool from high tide to low tide (0.31% at $S = 25.4$ and 0.93% at $S = 4.8$) would support freshwater inputs as well as rapid resuspension and mobilization of organic-rich surface sediments from the mangrove floor. Indeed, surface sediment (upper ~2 cm) of the adjacent mangrove had mean TOC level of 1.05% and POC:PN ratio of 8.7 (results from the previous study; Ray, Michaud, et al., 2018), similar to the water POC:TSM (0.41–0.93%) and POC:PN (~8–12) ratios at low tide. However, highly depleted value of δ^{13}POC at low tide

(approximately −38‰), neither matched with $\delta^{13}C$ of marine microalgae nor with $\delta^{13}C$ of mangrove plants. Regardless of the tide, persistent presence of lighter C in estuarine water, as evidenced from the highly negative residual $\Delta^{13}C$ (−42‰), was most likely due to the freshwater phytoplankton sources, in addition to methanogenic production (−62‰ in three occasions; Figure 8b) originating from the old mangroves (Ray, Michaud, et al., 2018).

Model calculations showed all ΔPOC values <1 (mean −27 ± 11 μM), suggesting perennial net removal of POC from the estuary and probably retention within the mangrove areas. This could be explained by the following: (1) High tree densities in FG mangroves (Proisy et al., 2007) could reduce water motion and particle outflux, while pneumatophores and complex root cables could trap significant amount of particulate material (litter, MPB, or phytoplankton) during the inundation phases (Hemminga et al., 1994; Middelburg & Nieuwenhuize, 1998). (2) Low MPB production under the trees and/or high grazing rates could reduce the amount of mangrove-derived POC available for export. (3) Leaf-litter consumption by crabs could greatly reduce the amount of mangrove-originated POC available for export (Andreetta et al., 2014; Kristensen, 2008). It is noteworthy that the pioneer and young mangroves of the Sinnamary estuary exhibited high bioturbation activities by benthic infauna (Aschenbroich et al., 2016) that could hamper the amount of POC exported as mangrove fresh leaves, litter, and MPB. (4) In addition to these local processes, POC import would be driven by huge TSM loads from the Amazon River. Furthermore, FG mangroves facing episodic erosional cycles, we assume that a sizeable fraction of the eroded sedimentary POC is re-imported into the mangrove system due to tidal currents. Walton et al. (2014) also reported POC inwelling in arid mangrove systems but for other reasons (inwelling of seagrass-derived POM and limited freshwater supply preventing particle flush). POC import to mangrove creeks was recognized by Santos et al. (2018) in subtropical environments. (5) Lastly, POC adsorption and flocculation, common in highly dynamic turbid estuaries like the Sinnamary (Jay & Musiak, 1994), would retain part of the mangrove-derived POC that reaches estuary during the ebb, nearby the mangrove area. It is also possible that lithogenic inputs from upstream could produce fast-sinking aggregates that settle on the estuarine bottoms.

4.3.3. Dissolved Inorganic Carbon

The DIC chemistry of the Sinnamary estuary in the dry season is largely controlled by pH decrease (17%) between high and low tide. Sea and river water mixing drives pH variations, as indicated by the strong linear positive correlation between pH and salinity ($r^2 = 0.95$). Other than endmember mixing, porewater inputs from the Sinnamary mud bank (pH 6.95), tidal flat (pH 6.85), and mangrove sediments (pH 5.99) also contribute to low surface water pH during low tide (our follow-up benthic study in November 2015; data not shown). High benthic mineralization of organic matter at low tide enhances pCO_2 release from the sediments to the overlying water, which is consistent with elevated pCO_2 at low tide, increasing water acidity. Porewater DIC concentration commonly reaches to 10 to 40 mM in the upper meter of the offshore mobile mud (Aller, 2004), which is much higher than the overlying water concentration measured in this study (0.45 to 1.34 mM). Two highly depleted peaks of $\delta^{13}DIC$ (−29.5‰ and −29.2‰) measured at low tide during the 24-hr survey were similar to the $\delta^{13}C$ signature of *Avicennia* plant material (−30.5‰ to −30.1‰) and indicative of the quasi exclusive (~97%) contribution of mangrove-derived OM inputs in the estuary (and subsequent OM respiration) via porewater drainage at low tide.

As total DIC increases, uncertainty on very small ΔC values increases (difference of two similar large numbers); thus, the residual isotopic components (Equation 4) were calculated only for DIC values <1 mM and ΔC > 1 (11 data in total). The introduction of very light isotopic components in DIC (similar to the isotopic signal of the POC pool), particularly at low salinity, would reflect freshwater phytoplankton or methane derived compounds as sources of remineralized carbon (mean $\Delta^{13}C = -55.7 \pm 15$‰; Figure 8c). Nonconservative DIC in the Tanzanian mangroves was attributed to OM mineralization in the intertidal areas and subsequent DIC export to the creeks (Bouillon et al., 2007). By contrast, heavy $\delta^{13}DIC$ at high tide would represent both phytoplankton uptake and CO_2 import from the ocean. Now, it is well documented for the mangrove systems that during ebb, porewaters can migrate into the water column and strongly increase DIC concentrations (Bouillon et al., 2007; Call et al., 2019; Volta et al., 2018). In this study, the pCO_2 values measured at low tide (~5,500 μatm) were sevenfold higher than those measured at high tide and 81% higher than the global average of pCO_2 in estuaries (3,033 ± 1,078 μatm; Chen et al., 2013). Porewater efflux rate depending on sediment permeability, pressure gradient, and bioturbation activities, numerous crab burrows in the

Sinnamary intertidal zone (Aschenbroich et al., 2016, 2017) would dramatically enhance hydraulic conductivity and porewater flushing to the tidal creeks (Stieglitz et al., 2013; Susilo & Ridd, 2005).

Estimates of air-water CO_2 fluxes (F_{CO2}) in the Sinnamary estuary highlighted the area as a significant regional source of CO_2 to the atmosphere in the dry season. Flux data generated from both models (Ho et al., 2016: 102 ± 81 mmol m^{-2} day^{-1}; Rosentreter et al., 2017: 157 ± 136 mmol m^{-2} day^{-1}) are comparable to global averages in mangrove estuaries (60 to 182 mmol m^{-2} day^{-1}; A. V. Borges et al., 2003; Bouillon et al., 2008) and the world's coastal seas (188 ± 70 mmol m^{-2} day^{-1}; Chen et al., 2013). However, regional F_{CO2} computed from wind speed parameterized piston velocities (k) in other tropical mangrove estuaries, like in Papua New Guinea, India, and Bahamas (mean of 43.6, 56, and 13.8 mmol m^{-2} day^{-1}, respectively; A. V. Borges et al., 2003), are lower than those calculated in this study. By contrast, Abril et al. (2005) applying floating chamber method and wind speed parametrized k reported much higher F_{CO2} (704–750 mmol m^{-2} day^{-1} at Salinity 0) downstream the Petit-Saut dam. The latter would be due to very high $pCO_{2(water)}$ (~10,000 μatm) recorded consistently at the riverine endmember by the authors. F_{CO2} computation depending on k estimates, more accurate estimates of the piston velocity in shallow-water estuarine systems are required to reduce uncertainties despite being a controversial approach (A. Borges et al., 2004).

Highest positive fluxes of DIC during the night and at sunrise (24-hr survey; Figure 9) could be linked to enhanced respiration. DIC export at low tide would primarily result from laterally driven benthic-emitted CO_2 that leads to elevated pCO_2 in the water and high CO_2 flux to the atmosphere. Inwelling water during the flood can import bicarbonates related to phytoplankton uptake to the mangroves, but it is more likely that CO_2 released during OM remineralization in the mobile muds is the main DIC source for FG mangroves. These mobile muds, belonging to the most extensive mud bank system of the planet, are "CO_2 reactors" (Aller, 1998, 2004). They may play a key role in sustaining mangrove development in FG and probably all along the northeast coast of South America under the Amazonian influence. By comparison, marine DIC import to the mangroves in the Danshui River estuary (West Taiwan) was assigned to the highly heterotrophic nature of the system and to DIC inputs from anthropogenic sources (Li et al., 2018). In most of other systems, net DIC export is observed through advective groundwater discharge or lateral transport of benthic CO_2 efflux (Call et al., 2019; Koné & Borges, 2008; Maher et al., 2013; Miyajima et al., 2009; Ray, Baum, et al., 2018; Santos et al., 2018; Taillardat et al., 2018). DIC import in some cases questions the existing global C budget where DIC export is considered as the main source of total C outwelling from the mangroves. More studies under different mangrove settings are required to reduce uncertainties due to data upscaling in order to re-evaluate the global C budget.

4.4. Carbon Fluxes in FG Mangroves and Elsewhere

Lack of salinity gradient during the time series survey in the wet season restricted the estimation of annual C exchanges. In the dry season, area-normalized DOC and POC fluxes during neap tides would strongly exceed the values reported for other mangroves worldwide (Ayukai et al., 1998; Dittmar et al., 2006; Dittmar & Lara, 2001; Ho et al., 2017; Romigh et al., 2006; Sippo et al., 2016; Twilley, 1985) but are comparable to few recent estimates (Li et al., 2018; Ray, Baum, et al., 2018). By contrast, DIC flux (0.90 g C m^{-2} day^{-1}) calculated in the Sinnamary during the dry season is lower than the "missing DIC" (~2.7 g C m^{-2} day^{-1}) in Maher et al. (2013) (Table 4) and one recent estimate in the Indian Sundarbans (2.4 g C m^{-2} day^{-1}; Ray, Baum, et al., 2018). In particular, DOC export estimate in the present study (8.1 g C m^{-2} day^{-1}) far exceeds (1 order of magnitude) the southern more Amazonia estuarine records (0.13–0.8 g C m^{-2} day^{-1}; Table 4) and ranges reported for tropical mangroves in Western Taiwan (1.52–4.0 g C m^{-2} day^{-1}; Li et al., 2018), Micronesia (0.09–0.42 g C m^{-2} day^{-1}; Call et al., 2019), and Indian Sundarbans (1.94 g C m^{-2} day^{-1}; Ray, Baum, et al., 2018), as well as subtropical Australian mangroves (0.05–5 g C m^{-2} day^{-1}; Maher et al., 2013; Santos et al., 2018). Higher DOC export from FG mangroves compared with the Brazilian records (Dittmar & Lara, 2001) could be linked to approximately six times lower water discharge and two times lower mean DOC concentration in the Caeté estuary, which is not under the influence of Amazonian waters. Such variability emphasizes hydrodynamics heterogeneity along the Brazil-FG coastlines. We hypothesize that FG mangroves could provide significant energy and metabolic substrates to aquatic consumers, through high DOC inputs, and sustain coastal water productivity.

Journal of Geophysical Research: Biogeosciences 10.1029/2020JG005739

Table 4
Global Values of Inorganic and Organic Carbon Export (in g C m^{-2} day^{-1}) From Mangrove Dominated Estuaries/Creeks From the Literature and This Study

Location	Mangrove settings, tidal regime	Season year	Total OC flux g C m^{-2} day^{-1}	DOC flux g C m^{-2} day^{-1}	POC flux g C m^{-2} day^{-1}	DIC flux g C m^{-2} day^{-1}	Methods	References
Sinnamary estuary French Guiana	Riverine Fringe Tide dominated Tidal ht. = 2–3 m (NT)	Dry 2015	6.79	8.14	−1.35	−0.90	24-hr study DEM approach	This study
Amazon River *Furo de Meio* Brazil	Riverine Fringe Tide dominated Tidal ht. = 4–5 m (ST)	Dry, wet 1996–97	0.65	0.13	0.09	—	36 tidal cycles Eulerian approach	Dittmar and Lara (2001)
Caeté Coast, Brazil	Riverine Fringe Tide dominated Tidal ht. = 4 m (ST)	Dry, 2001	—	0.37	—	—	Pore water DOM degradation experiment	Dittmar et al. (2006)
Rookery Bay, Florida	Two basin mangroves River dominated Tidal ht. = 0.5 m (mean)	Dry, wet 1979	0.045–0.05	Bay forest 0.035 Creek forest 0.042	Bay forest 0.01 Creek forest 0.042	—	Flume constructed across tidal creeks	Twilley (1985)
Shark River[a, b] Florida	Riverine Everglades River dominated Tidal ht. = 0.5–1 m	[a]Dry, wet 2003	—	0.15[a]	—	0.56—0.72[b]	[a]Flume study	[a]Romigh et al. (2006)
		[b]Wet 2010		0.06–0.08[b]			[b]Isotopic mass eqn.	[b]Ho et al. (2017)
Coral, Conn Creek NE Australia	Tide dominated	Dry, wet 1996–1997	—	0.16	~0.06	—	Eulerian method, Eddy diffusion	Ayukai et al., 1998
Moreton Bay East Australia	Tide dominated Tidal ht. = 1–2 m (ST)	Winter, summer 2011–2012	—	0.13–0.49	—	2.2–4.1	Airborne laser survey DEM and ArcGIS	Maher et al. (2013)
North East South Australian coasts	Six pristine mangrove creeks, tide dominate Tidal ht. = 0.7–4.8 m	Wet, 2014	—	—	—	0.26–1.02	24-hr study DEM and ArcGIS	Sippo et al. (2016)
Fly Delta Papua New Guinea	River dominated Tidal ht. = 1–2 m	1991–1993	—	—	0.78	—	Litter removal by crabs	Robertson and Alongi (1995)
Western Taiwan	Four mangrove estuaries Tide dominated Tidal ht. = 1–4 m (ST)	Dry, wet 2011–2014	2.09–9.79	1.52–4.0	0.57–5.8	1.45–4.45	Concentration gradient method	Li et al. (2018)
Indian Sundarbans	Saptamukhi estuary Tide dominated Tidal ht = 3–5 m (ST)	Winter, 2014	2.32	1.94	0.37	2.42	Time series Mass based method	Ray, Baum, et al. (2018)
Evans Head, Australia	Mangrove salt marsh tidal creek	Dry, wet 2012–2013	0.04	0.05	−0.012	0.07–0.22	25-hr time series Eulerian approach	Santos et al. (2018)
Palau, Micronesia Volcanic island	Two mangrove creeks Tide dominated Tidal ht = 2 m (ST)	Wet, 2015	0.1–0.61	0.09–0.42	0.01–0.19	0.12–0.95	24-hr time series Eulerian approach	Call et al. (2019)

Note. Negative values from our study indicate import fluxes of POC and DIC. ST = spring tide; NT = neap tide.
[a]Romigh et al. (2006).
[b]Ho et al. (2017).

Integrating the two seasons at annual scale, estimates of Sinnamary estuarine exchanges of surface water DOC, POC, and DIC to the Atlantic coastal waters are 87 ± 52, 16 ± 12, and 21 ± 15 Gg C year^{-1}, respectively. Maximum values for each C component occur during the wet season. Estimated mean flux of total organic carbon (TOC = DOC + POC) is 3.7 times higher than previously reported export flux of TOC, whereas it is similar for DIC (based on two sampling points downstream Sinnamary in 2003; Abril et al., 2005) and comparable to total carbon export estimated in 2003 downstream the Petit-Saut dam (80 Gg C year^{-1}; de Junet, 2004). Since river flow data obtained from DEAL Guyane-EDF did not cover the whole month of June 2015 (700 m^3 s^{-1} during the first forecast), these values could change depending on water flow controlled by seasonal rainfalls and dam-regulated water discharges. In this study, mangrove-derived export flux of surface water DOC (33.7 Gg C year^{-1}) would be equivalent to 38% of the average Sinnamary riverine/estuarine DOC export flux. Huang et al. (2012) estimated worldwide mangrove contribution to the tropical riverine DOC discharge to be 17%, which is smaller than our regional estimates in French Guiana. Total DOC export from the Sinnamary estuarine surface water and associated mangroves to the Atlantic Ocean would be 120.7 Gg C year^{-1}.

As already mentioned, present mangrove-derived flux data, solely based on dry season time series and neap tide conditions, may not allow extrapolating on annual scale. The same is true for the annual estuarine export calculation. Higher values of all three carbon forms at Station D (mean DOC, POC, and DIC concentrations: 758 ± 98, 22 ± 7, and 829 ± 252 μM, respectively) can be explained by direct mangrove and mud bank influences. At Station W, higher freshwater dilution reduced dissolved C concentrations (528 ± 62, 136 ± 89, and 176 ± 81 μM for DOC, POC, and DIC, respectively). Clearly, seasonal data collection and multiple time series studies conducted in various sites are required to improve C fluxes resolution (Sippo et al., 2016). Because of the prominent halocline observed in the Sinnamary water column during the wet season, further recommendation would be to include bottom water data into C flux calculations.

5. Conclusion

This study examined the temporal variability of DOC, POC, and DIC compositions and exchange fluxes in the mangrove-dominated Sinnamary estuary (French Guiana) under Amazonian influence. Tidal factors mainly governed the sources and exchanges of OC (DOC and POC), whereas benthic remineralization controlled DIC exchange fluxes. However, the magnitude of C exchange fluxes is very uncertain, due to variability in tidal (spring vs. neap) and seasonal (wet vs. dry) patterns, a stratified water column with different water masses and C concentrations, and differences between sampling sites (creeks vs. estuarine gradient). Clearly, both spatial and temporal heterogeneities of stocks and fluxes can hamper a "real" estimate of annual global C budget. We do agree with Maher et al. (2013) and Ho et al. (2017) stating that global C budget estimates for worldwide mangroves would require performing biogeochemical studies at seasonal scale in a range of mangrove systems along the latitudinal gradient, with different environmental forcing, species composition, and litter export, to constrain the magnitude and drivers of DOC, POC, and DIC exchange fluxes.

Data Availability Statement

Data for this study have been deposited in a general data repository (https://figshare.com/articles/DS01_RR_xlsx/11971974).

Acknowledgments

R. Ray is indebted to Labex MER International Postdoctoral Program for providing fellowship (FNP150009-DOCT-RAY). Part of this work was cofunded by the French Research National Agency under the programs "Young researcher" (BIOMANGO: ANR-12-JSV7-0012-01) and "Programme Investissements d'Avenir" (Labex Mer: ANR-10-LABX-19 and Labex CEBA: ANR-10-LABX-25-01). It was also supported by the CNRS (PEPS Mangrove and PIG programs). Authors thank O. Lebeau (PSO, UMS 3113, IUEM, Plouzané) and I. Klingensmith (SOMAS, New York) for their help in the laboratory work. S. Ruehlow and I. Hilke (Max Planck Institute for Biogeochemistry, Jena) are acknowledged for measuring δ^{13}DOC and DOC, respectively. The authors are in debt to J. Printemps (Sinnamary), E. Marcon and V. Troispoux (ECOFOG, Kourou), and M. Brossard and M. Sarrazin (IRD, Cayenne) for their logistic help during field work. S. Bouillon (Katholieke Universiteit Leuven) and R. C. Aller (Stony Brook University, New York) are gratefully acknowledged for their scientific inputs and for editing on earlier version of the manuscript. The Editor and Reviewers are sincerely thanked for their constructive comments and useful edits. This paper is a GDR LIGA contribution.

References

Abril, G., Guérin, F., Richard, S., Delmas, R., Galy-Lacaux, C., Gosse, P., et al. (2005). Carbon dioxide and methane emissions and the carbon budget of a 10-year old tropical reservoir (Petit-Saut, French Guiana). *Global Biogeochemical Cycles*, *19*, GB4007. https://doi.org/10.1029/2005GB002457

Adame, M. E., & Lovelock, C. E. (2011). Carbon and nutrient exchange of mangrove forests with the coastal ocean. *Hydrobiologia*, *663*(1), 23–50. https://doi.org/10.1007/s10750-010-0554-7

Aller, R. C. (1998). Mobile deltaic and continental shelf muds as fluidized bed reactors. *Marine Chemistry*, *61*(3–4), 143–155. https://doi.org/10.1016/S0304-4203(98)00024-3

Aller, R. C. (2004). Conceptual models of early diagenetic processes: The muddy seafloor as an unsteady, batch reactor. *Journal of Marine Research*, *62*(6), 815–835. https://doi.org/10.1357/0022240042880837

Aller, R. C., & Blair, N. E. (2006). Carbon remineralization in the Amazon-Guianas tropical mobile mudbelt: A sedimentary incinerator. *Continental Shelf Research*, *26*(17–18), 2241–2259. https://doi.org/10.1016/j.csr.2006.07.016

Allison, M. A., Lee, M. T., Ogston, A. S., & Aller, R. C. (2000). Origin of Amazon mudbanks along the northeastern coast of South America. *Marine Geology*, *163*(1–4), 241–256. https://doi.org/10.1016/S0025-3227(99)00120-6

Alongi, D. M. (2014). Carbon cycling and storage in mangrove forests. *Annual Review of Marine Science*, *6*(1), 195–219. https://doi.org/10.1146/annurev-marine-010213-135020

Andreetta, A., Fusi, M., Cameldi, I., Cimò, F., Carnicelli, S., & Cannicci, S. (2014). Mangrove carbon sink. Do burrowing crabs contribute to sediment carbon storage? Evidence from a Kenyan mangrove system. *Journal of Sea Research*, *85*, 524–533. https://doi.org/10.1016/j.seares.2013.08.010

Anthony, E. J., Dolique, F., Gardel, A., Gratiot, N., Proisy, C., & Polidori, L. (2008). Nearshore intertidal topography and topographic-forcing mechanisms of an Amazon-derived mud bank in French Guiana. *Continental Shelf Research*, *28*(6), 813–822. https://doi.org/10.1016/j.csr.2008.01.003

Anthony, E. J., Gardel, A., Gratiot, N., Proisy, C., Allison, M. A., Dolique, F., & Fromard, F. (2010). The Amazon-influenced muddy coast of South America: A review of mud-bank-shoreline interactions. *Earth-Science Reviews*, *103*(3–4), 99–121. https://doi.org/10.1016/j.earscirev.2010.09.008

Aschenbroich, A., Michaud, E., Gilbert, F., Fromard, F., Alt, A., Le Garrec, V., et al. (2017). Bioturbation functional roles associated with mangrove development in French Guiana, South America. *Hydrobiologia*, *794*(1), 179–202. https://doi.org/10.1007/s10750-017-3093-7

Aschenbroich, A., Michaud, E., Stieglitz, T., Fromard, F., Gardel, A., Tavares, M., & Thouzeau, G. (2016). Brachyuran crab community structure and associated sediment reworking activities in pioneer and young mangroves of French Guiana, South America. *Estuarine, Coastal and Shelf Science*, *182*, 60–71. https://doi.org/10.1016/j.ecss.2016.09.003

Ayukai, T., Miller, D., Wolanski, E., & Spagnol, S. (1998). Fluxes of nutrients and dissolved and particulate organic carbon in two mangrove creeks in northeastern Australia. *Mangroves and Salt Marshes*, *2*(4), 223–230. https://doi.org/10.1023/A:1009923410116

Betoulle, J. L., Fromard, F., Fabre, A., & Puig, H. (2001). Caractérisation des chutes de litière et des apports au sol en nutriments dans une mangrove de Guyane française. *Canadian Journal of Botany*, *79*, 238–249.

Borges, A., Delille, B., Schiettecatte, L.-S., Gazeau, F., Abril, G., & Frankignoulle, M. (2004). Gas transfer velocities of CO_2 in three European estuaries (Randers Fjord, Scheldt and Thames). *Limnology and Oceanography*, *49*(5), 1630–1641. https://doi.org/10.4319/lo.2004.49.5.1630

Borges, A. V., Djenidi, S., Lacroix, G., The'ate, J., Delille, B., & Frankignoulle, M. (2003). Atmospheric CO_2 flux from mangrove surrounding waters. *Geophysical Research Letters*, *30*(11), 1558. https://doi.org/10.1029/2003GL017143

Bouillon, S., Borges, A. V., Castañeda-Moya, E., Diele, K., Dittmar, T., Duke, N. C., et al. (2008). Mangrove production and carbon sinks: A revision of global budget estimates. *Global Biogeochemical Cycles*, *22*, GB2013. https://doi.org/10.1029/2007GB003052

Bouillon, S., Middelburg, J. J., Dehairs, F., Borges, A. V., Abril, G., Flindt, M. R., et al. (2007). Importance of intertidal sediment processes and porewater exchange on the water column biogeochemistry in a pristine mangrove creek (Ras Dege, Tanzania). *Biogeosciences*, *4*(3), 311–322. https://doi.org/10.5194/bg-4-311-2007

Buchmann, N., Guehl, J.-M., Barigah, T. S., & Ehleringer, J. R. (1997). Inter-seasonal comparison of CO_2 concentrations, isotopic composition, and carbon dynamics in an Amazonian rainforest (French Guiana). *Oecologia*, *110*(1), 120–131. https://doi.org/10.1007/s004420050140

Call, M., Sanders, C. J., Macklin, P. A., Santos, I. R., & Maher, D. T. (2019). Carbon outwelling and emissions from two contrasting mangrove creeks during the monsoon storm season in Palau, Micronesia. *Estuarine, Coastal and Shelf Science*, *218*, 340–348. https://doi.org/10.1016/j.ecss.2019.01.002

Cawley, K. M., Yamashita, Y., Maie, N., & Jaffé, R. (2013). Using optical properties to quantify fringe mangrove inputs to the Dissolved Organic Matter (DOM) pool in a subtropical estuary. *Estuaries and Coasts*, *37*, 399–410.

Chen, C. T. A., Huang, T. H., Chen, Y. C., Bai, Y., He, X., & Kang, Y. (2013). Air-sea exchanges of CO_2 in the world's coastal seas. *Biogeosciences*, *10*(10), 6509–6544. https://doi.org/10.5194/bg-10-6509-2013

Cifuentes, L. A., Coffin, R. B., Solorzano, L., Cardenas, W., Espinoza, J., & Twilley, R. R. (1996). Isotopic and elemental variations of carbon and nitrogen in a mangrove estuary. *Estuarine, Coastal and Shelf Science*, *43*(6), 781–800. https://doi.org/10.1006/ecss.1996.0103

Condie, S. A. (1991). Separation and recirculation of the North Brazil Current. *Journal of Marine Research*, *49*(1), 1–19. https://doi.org/10.1357/002224091784968620

de Junet, A. (2004). Etude qualitative de la matière organique particulaire dans le réservoir de Petit-Saut (Guyane Française): Composition Isotopique (δ13C), élémentaire (C/N) et pigmentaire. Master report, Talence, pp 41.

de Rezende, C. E., Lacerda, L. D., Ovalle, A. R. C., & Silva, L. F. F. (2007). Dial organic carbon fluctuations in a mangrove tidal creek in Sepetiba bay, Southeast Brazil. *Brazllian Journal of Biology*, *67*(4), 673–680. https://doi.org/10.1590/S1519-69842007000400012

Dickson, A. G., & Millero, F. J. (1987). A comparison of the equilibrium constants for the dissociation of carbonic acid in seawater media. *Deep Sea Research Part A: Oceanographic Research Papers*, *34*, 1733–1743.

Dittmar, T., Hertkorn, N., Kattner, G., & Lara, R. J. (2006). Mangroves, a major source of dissolved organic carbon to the oceans. *Global Biogeochemical Cycles*, *20*, GB1012. https://doi.org/10.1029/2005GB002570

Dittmar, T., & Lara, R. J. (2001). Do mangroves rather than rivers provide nutrients to coastal environments south of the Amazon River? Evidence from long-term flux measurements. *Marine Ecology Progress Series*, *213*, 67–77. https://doi.org/10.3354/meps213067

Forest, K., Wan, P., & Preston, C. M. (2004). Catechin and hydroxybenzhydrols as models for the environmental photochemistry of tannins and lignins. *Photochemistry and Photobiology*, *3*(5), 463–472. https://doi.org/10.1039/b402241f

Fromard, F., Puig, H., Mougin, E., Marty, G., Betoulle, J. L., & Cadamuro, L. (1998). Structure, above-ground biomass and dynamics of mangrove ecosystems: New data from French Guiana. *Oecologia*, *115*(1–2), 39–53. https://doi.org/10.1007/s004420050489

Fromard, F., Vega, C., & Proisy, C. (2004). Half a century of dynamic coastal change affecting mangrove shorelines of French Guiana. A case study based on remote sensing data analyses and field surveys. *Marine Geology*, *208*(2–4), 265–280. https://doi.org/10.1016/j.margeo.2004.04.018

Gardel, A., & Gratiot, N. (2005). A satellite image-based method for estimating rates of mud bank migration, French Guiana, South America. *Journal of Coastal Research*, *21*, 720–728.

Giri, C., Ochieng, E., Tieszen, L. L., Zhu, Z., Singh, A., Loveland, T., et al. (2011). Status and distribution of mangrove forests of the world using Earth observation satellite data. *Global Ecology and Biogeography*, *20*(1), 154–159. https://doi.org/10.1111/j.1466-8238.2010.00584.x

Gontharet, S., Mathieu, O., Lévêque, J., Lesourd, S., Caillaud, J., Gardel, A., et al. (2014). Distribution and sources of bulk organic matter (OM) on a tropical intertidal mud bank in French Guiana from elemental and isotopic proxies. *Chemical Geology*, *376*, 1–10. https://doi.org/10.1016/j.chemgeo.2014.03.009

Hansson, I. (1973). A new set of acidity constants for carbonic acid and boric acid in seawater. *Deep Sea Research*, *20*, 461–478.

Hemminga, M. A., Slim, F. J., Kazungu, J., Ganssen, G. M., Nieuwenhuize, J., & Kruyt, N. M. (1994). Carbon outwelling from a mangrove forest with adjacent seagrass beds and coral reefs (Gazi Bay, Kenya). *Marine Ecology Progress Series*, *106*, 291–301. https://doi.org/10.3354/meps106291

Hernes, P. J., Benner, R., Cowie, G. L., Goni, M. A., Bergamaschi, B. A., & Hedges, J. I. (2001). Tannin diagenesis in mangrove leaves from a tropical estuary: A novel molecular approach. *Geochimica Cosmochima Acta*, *65*(18), 3109–3122. https://doi.org/10.1016/S0016-7037(01)00641-X

Ho, D. T., Coffineau, N., Hickman, B., Chow, N., Koffman, T., & Schlosser, P. (2016). Influence of current velocity and wind speed on air-water gas exchange in a mangrove estuary. *Geophysical Research Letters*, *43*, 3813–3821. https://doi.org/10.1002/2016GL068727

Ho, D. T., Ferrón, S., Engel, V. C., Anderson, W. T., Swart, P. K., Price, R. M., & Barbero, L. (2017). Dissolved carbon biogeochemistry and export in mangrove dominated rivers of the Florida Everglades. *Biogeosciences*, *14*(9), 2543–2559. https://doi.org/10.5194/bg-14-2543-2017

Huang, T. H., Fu, Y. H., Pan, P. Y., & Chen, C. T. A. (2012). Fluvial carbon fluxes in tropical rivers. *Current Opinion in Environment Sustainability*, *4*(2), 162–169. https://doi.org/10.1016/j.cosust.2012.02.004

Jay, D. A., & Musiak, J. D. (1994). Particle trapping in estuarine tidal flows. *Journal of Geophysical Research*, *99*(C10), 20,445–20,461. https://doi.org/10.1029/94JC00971

Jennerjahn, T. C., & Ittekkot, V. (2002). Relevance of mangroves for the production and deposition of organic matter along tropical continental margins. *Die Naturwissenschaften*, *89*(1), 23–30. https://doi.org/10.1007/s00114-001-0283-x

Koné, Y. J.-M., & Borges, A. V. (2008). Dissolved inorganic carbon dynamics in the waters surrounding forested mangroves of the Ca Mau Province (Vietnam). *Estuarine, Coastal and Shelf Science*, *77*(3), 409–421. https://doi.org/10.1016/j.ecss.2007.10.001

Kristensen, E. (2008). Mangrove crabs as ecosystem engineers; with emphasis on sediment processes. *Journal of Sea Research*, *59*(1–2), 30–43. https://doi.org/10.1016/j.seares.2007.05.004

Kristensen, E., Bouillon, S., Dittmar, T., & Marchand, C. (2008). Organic carbon dynamics in mangrove ecosystems: A review. *Aquatic Botany*, *89*(2), 201–219. https://doi.org/10.1016/j.aquabot.2007.12.005

Kristensen, E., & Suraswadi, P. (2002). Carbon, nitrogen and phosphorus dynamics in creek water of a southeast Asian mangrove forest. *Hydrobiologia*, *474*(1/3), 197–211. https://doi.org/10.1023/A:1016544006720

Lee, S. Y., Primavera, J. H., Dahdouh-Guebas, F., McKee, K., Bosire, J. O., Cannicci, S., et al. (2014). Ecological role and services of tropical mangrove ecosystems: A reassessment. *Global Ecology and Biogeography*, *23*(7), 726–743. https://doi.org/10.1111/geb.12155

Lewis, E., & Wallace, D. W. R. (1998). *Program developed for CO_2 system calculations*. Oak Ridge, Tenn: Carbon Dioxide Information Analysis Center, Oak Ridge National Laboratory.

Li, S.-B., Chen, P.-H., Huang, J.-S., Hsueh, M.-L., Hsieh, L.-Y., Lee, C.-L., & Lin, H.-J. (2018). Factors regulating carbon sinks in mangrove ecosystems. *Global Change Biology*, *24*(9), 4195–4210. https://doi.org/10.1111/gcb.14322

Maher, D. T., Santos, I. R., Golsby-Smith, L., Gleeson, J., & Eyre, B. D. (2013). Groundwater-derived dissolved inorganic and organic carbon exports from a mangrove tidal creek: The missing mangrove carbon sink? *Limnology and Oceanography*, *58*(2), 475–488. https://doi.org/10.4319/lo.2013.58.2.0475

Marchand, C. (2017). Soil carbon stocks and burial rates along a mangrove forest chronosequence (French Guiana). *Forest Ecology and Management*, *384*, 92–99. https://doi.org/10.1016/j.foreco.2016.10.030

Marchand, C., Baltzer, F., Lallier-Vergès, E., & Albéric, P. (2004). Interstitial water chemistry in mangrove sediments in relationship to species composition and developmental stage. (French Guiana). *Marine Geology*, *208*(2–4), 361–381. https://doi.org/10.1016/j.margeo.2004.04.015

Martinez, J. M., Guyot, J. L., Filizola, N., & Sondag, F. (2009). Increase in suspended sediment discharge of the Amazon River assessed by monitoring network and satellite data. *Catena*, *79*(3), 257–264. https://doi.org/10.1016/j.catena.2009.05.011

Middelburg, J. J., & Nieuwenhuize, J. (1998). Carbon and nitrogen stable isotopes in suspended matter and sediments from the Schelde estuary. *Marine Chemistry*, *60*(3–4), 217–225. https://doi.org/10.1016/S0304-4203(97)00104-7

Mitchell, B. G., Kahru, M., Wieland, J., & Stramska, M. (2002). Determination of spectral absorption coefficients of particles, dissolved material and phytoplankton for discrete water samples. In J. L. Mueller, G. D. Fargion, & C. R. McClain (Eds.), *Ocean optics protocols for satellite ocean color sensor validation* (Chap. 12, pp. 125–153). Greenbelt, MD: NASA Goddard Space Flight Center.

Miyajima, T., Tsuboi, Y., Tanaka, Y., & Koike, I. (2009). Export of inorganic carbon from two Southeast Asian mangrove forests to adjacent estuaries as estimated by the stable isotope composition of dissolved inorganic carbon. *Journal of Geophysical Research*, *114*, G01024. https://doi.org/10.1029/2008JG000861

Mook, W. G., & Tan, T. C. (1991). Stable carbon isotopes in rivers and estuaries. In E. T. Degens, S. Kempe, & J. E. Richey (Eds.), *Biogeochemistry of Major World Rivers* (pp. 245–264). Chichester: SCOPE, John Wiley and Sons Ltd.

Mori, C., Santos, I. R., Brumsack, H.-J., Schnetger, B., Dittmar, T., & Seidel, M. (2019). Non-conservative behavior of dissolved organic matter and trace metals (Mn, Fe, Ba) driven by porewater exchange in a subtropical mangrove-estuary. *Frontiers in Marine Science*, *6*, 481. https://doi.org/10.3389/fmars.2019.00481

Odum, W. E., & Heald, E. J. (1975). The detritus-band food web on an estuarine mangrove community. In L. L. Cromin (Ed.), *Estuarine research* (pp. 265–286). New York: Academic press.

Officer, C. B. (1976). *Physical oceanography of estuaries (and associated coastal waters)* (p. 465). New York: Wiley-Inter science.

Parra, M., & Pujos, M. (1998). Origin of late Holocene fine grained sediments on the French Guiana Shelf. *Continental Shelf Research*, *18*, 1613–1629.

Proisy, C., Couteron, P., & Fromard, F. (2007). Predicting and mapping mangrove biomass from canopy grain analysis using Fourier-based textural ordination of IKONOS images. *Remote Sensing of Environment*, *109*(3), 379–392. https://doi.org/10.1016/j.rse.2007.01.009

Proisy, C., Gratiot, N., Anthony, E., Gardel, A., Fromard, F., & Heuret, P. (2009). Mud bank colonization by opportunistic mangroves: A case study from French Guiana using Lidar data. *Continental Shelf Research*, *29*(3), 632–641. https://doi.org/10.1016/j.csr.2008.09.017

Ray, R., Baum, A., Gleixner, G., Rixen, T., & Jana, T. K. (2018). Exportation of dissolved (inorganic and organic) and particulate carbon from mangroves and their implications to the carbon budget in the Indian Sundarbans. *Science of the Total Environment*, *621*, 535–547. https://doi.org/10.1016/j.scitotenv.2017.11.225

Ray, R., Michaud, E., Aller, R. C., Vantrepotte, V., Gleixner, G., Walcker, R., et al. (2018). Sources and distribution of carbon (DOC, POC, DIC) in a mangrove dominated estuary (French Guiana, South America). *Biogeochemistry*, *138*(3), 297–321. https://doi.org/10.1007/s10533-018-0447-9

Raymond, P. A., & Cole, J. J. (2001). Gas exchange in rivers and estuaries: Choosing a gas transfer velocity. *Estuaries*, *24*, 269–274.

Robertson, A. I., & Alongi, D. M. (1995). Role of riverine mangrove forest in organic carbon export to the tropical coastal ocean: A preliminary mass balance for the Fly Delta (Papua New Guinea). *Geo-Marine Letters*, *15*(3–4), 134–139. https://doi.org/10.1007/BF01204454

Romera-Castillo, C., Sarmento, H., Alvarez-Salgado, X. A., Gasol, J. M., & Marrase, C. (2010). Production of chromophoric dissolved organic matter by marine phytoplankton. *Limnology and Oceanography*, *55*(1), 446–454. https://doi.org/10.4319/lo.2010.55.1.0446

Romigh, M. A., David, S. E., Rivera-Monroy, V. H., & Twilley, R. R. (2006). Flux of organic carbon in a riverine mangrove wetland in the Florida coastal Everglades. *Hydrobiology*, *569*(1), 505–516. https://doi.org/10.1007/s10750-006-0152-x

Rosentrater, J. A., Maher, D. T., Ho, D. T., Call, M., Barr, J. G., & Eyre, B. D. (2017). Spatial and temporal variability of CO_2 and CH_4 gas transfer velocities and quantification of the CH4 microbubble flux in mangrove dominated estuaries. *Limnology and Oceanography*, *62*(2), 561–578. https://doi.org/10.1002/lno.10444

Santos, I. R., Maher, D. M., Larkin, R., Webb, J. R., & Sanders, C. J. (2018). Carbon outwelling and outgassing vs. burial in an estuarine tidal creek surrounded by mangrove and saltmarsh wetlands. *Limnology and Oceanography*, *9999*, 1–18.

Sarazin, G., Michard, G., & Prévot, F. M. P. (1999). A rapid and accurate spectroscopic method for alkalinity measurements in sea water samples. *Water Research*, *33*(1), 290–294. https://doi.org/10.1016/S0043-1354(98)00168-7

Scheibe, A., Krantz, L., & Gleixner, G. (2012). Simultaneous determination of the quantity and isotopic signature of dissolved organic matter from soil water using high-performance liquid chromatography/isotope ratio mass spectrometry. *Rapid Communications in Mass Spectrometry*, *26*(2), 173–180. https://doi.org/10.1002/rcm.5311

Schwendenmann, L., & Veldkamp, E. (2006). Long-term CO2 production from deeply weathered soils of a tropical rain forest: Evidence for a potential feedback to climate warming. *Global Change Biology*, *12*, 1–16.

Shank, G. C., Lee, R., Vähätalo, A. V., Zepp, R. G., & Bartels, E. (2010). Production of chromophoric dissolved organic matter from mangrove leaf litter and floating Sargassum colonies. *Marine Chemistry*, *119*(1–4), 172–181. https://doi.org/10.1016/j.marchem.2010.02.002

Sippo, J. Z., Maher, D. T., Tait, D. R., Holloway, C., & Santos, I. R. (2016). Are mangroves drivers or buffers of coastal acidification? Insights from alkalinity and dissolved inorganic carbon export estimates across a latitudinal transect. *Global Biogeochemical Cycles*, *30*, 753–766. https://doi.org/10.1002/2015GB005324

Stieglitz, T. C., Clark, J. F., & Hancock, G. J. (2013). The mangrove pump: The tidal flushing of animal burrows in a tropical mangrove forest determined from radionuclide budgets. *Geochimica et Cosmochimica Acta*, *102*, 12–22. https://doi.org/10.1016/j.gca.2012.10.033

Strickland, J. D. H., & Parsons, T. R. (1968). *A practical handbook of seawater analysis*, *Fisheries Research Board of Canada 167* (p. 293). Ottawa: Fisheries Research Board of Canada.

Susilo, A., & Ridd, P. V. (2005). The bulk hydraulic conductivity of mangrove soil perforated with animal burrows. *Wetlands Ecology and Management*, *13*(2), 123–133. https://doi.org/10.1007/s11273-004-8324-9

Taillardat, P., Ziegler, A. D., Friess, D. A., Widory, D., Van Truong, V., David, F., et al. (2018). Carbon dynamics and inconstant porewater input in a mangrove tidal creek over contrasting seasons and tidal amplitudes. *Geochimica et Cosmochimica Acta*, *237*, 32–48. https://doi.org/10.1016/j.gca.2018.06.012

Takahashi, T., Sutherland, S. C., Wanninkoff, R., Sweeney, C., Feely, R. A., Chipman, D. W., et al. (2009). Climatological mean and decadal change in surface ocean pCO_2, and net sea-air CO_2 flux over the global oceans. *Deep Sea Research, Part II*, *56*(8–10), 554–577. https://doi.org/10.1016/j.dsr2.2008.12.009

Twilley, R. (1985). The exchange of organic carbon in basin mangrove forests in a southwest Florida estuary. *Estuarine, Coastal and Shelf Science*, *20*(5), 543–557. https://doi.org/10.1016/0272-7714(85)90106-4

Volta, H., Friederich, G., Engel, V., & Bhat, M. (2018). Influence of water management and natural variability on dissolved inorganic carbon dynamics in a mangrove-dominated estuary. *Science of the Total Environment*, *635*, 479–486. https://doi.org/10.1016/j.scitotenv.2018.04.088

Walcker, R., Gandois, L., Proisy, C., Corenblit, D., Mougin, É., Ray, R., & Fromard, F. (2018). Control of "blue carbon" storage by mangrove ageing: Evidence from a 66-year-chronosequence in French Guiana. *Global Change Biology*, *24*(6), 2325–2338. https://doi.org/10.1111/gcb.14100

Walton, M. E. M., Al-Maslamani, I., Skov, M. W., Al-Shaikh, I., Al-Ansari, I. S., Kennedy, H. A., & Vay, L. L. (2014). Outwelling from arid mangrove systems is sustained by inwelling of seagrass productivity. *Marine Ecology Progress Series*, *507*, 125–137. https://doi.org/10.3354/meps10827

Wanninkhof, R. H. (1992). Relationship between wind speed and gas exchange over the ocean. *Journal of Geophysical Research*, *97*(C5), 7373–7382. https://doi.org/10.1029/92JC00188

Watanabe, K., & Kuwae, T. (2015). How organic carbon derived from multiple sources contributes to carbon sequestration processes in a shallow coastal system? *Global Change Biology*, *21*(7), 2612–2623. https://doi.org/10.1111/gcb.12924

Weiss, R. (1974). Carbon dioxide in water and seawater: The solubility of a non-ideal gas. *Marine Chemistry*, *2*(3), 203–215. https://doi.org/10.1016/0304-4203(74)90015-2

Woodroffe, C. (1992). Mangrove sediments and geomorphology. In *Tropical mangrove ecosystems* (Chap. 2, p. 329). Washington, USA: John Wiley & Sons, American Geo-physical Union.